Scientific Reports

https://doi.org/10.1038/s41598-026-39640-y

Article in Press

Electrochemically optimized multi-component polyacrylonitrile nanofiber scaffolds as a platform for three-dimensional glioblastoma cell culture

Received: 18 November 2025

Accepted: 6 February 2026

Published online: 09 March 2026

Cite this article as: Kurt Ş., Bal Altuntaş D., Sevim Nalkıran H. *et al.* Electrochemically optimized multi-component polyacrylonitrile nanofiber scaffolds as a platform for three-dimensional glioblastoma cell culture. *Sci Rep* (2026). https://doi.org/10.1038/s41598-026-39640-y

Şeymanur Kurt, Derya Bal Altuntaş, Hatice Sevim Nalkıran, Sema Aslan, Çağdaş Koçak, Atilla Eren Mamuk & İhsan Nalkıran

We are providing an unedited version of this manuscript to give early access to its findings. Before final publication, the manuscript will undergo further editing. Please note there may be errors present which affect the content, and all legal disclaimers apply.

If this paper is publishing under a Transparent Peer Review model then Peer Review reports will publish with the final article.

ARTICLE IN PRESS

© The Author(s) 2026. **Open Access** This article is licensed under a Creative Commons Attribution-NonCommercial-NoDerivatives 4.0 International License, which permits any non-commercial use, sharing, distribution and reproduction in any medium or format, as long as you give appropriate credit to the original author(s) and the source, provide a link to the Creative Commons licence, and indicate if you modified the licensed material. You do not have permission under this licence to share adapted material derived from this article or parts of it. The images or other third party material in this article are included in the article's Creative Commons licence, unless indicated otherwise in a credit line to the material. If material is not included in the article's Creative Commons licence and your intended use is not permitted by statutory regulation or exceeds the permitted use, you will need to obtain permission directly from the copyright holder. To view a copy of this licence, visit http://creativecommons.org/licenses/by-nc-nd/4.0/.

ARTICLE IN PRESS

Electrochemically Optimized Multi-Component Polyacrylonitrile Nanofiber Scaffolds as a Platform for Three-Dimensional Glioblastoma Cell Culture

Şeymanur Kurt[1], Derya Bal Altuntaş[2], Hatice Sevim Nalkıran[3], Sema Aslan[4], Çağdaş Koçak[5], Atilla Eren Mamuk[5], İhsan Nalkıran[3]*

[1] Department of Advanced Technologies, Institute of Graduate Studies, Recep Tayyip Erdogan University, Rize 53100, Türkiye

[2]* Department of Bioengineering, Faculty of Engineering and Architecture, Recep Tayyip Erdogan University, Rize 53100, Türkiye

[3] Department of Medical Biology, Faculty of Medicine, Recep Tayyip Erdogan University, Rize 53100, Türkiye

[4] Department of Chemistry, Faculty of Science, Mugla Sitki Kocman University, Muğla 48100, Türkiye

[5] Department of Physics, Faculty of Science, Mugla Sitki Kocman University, Muğla 48100, Türkiye

*Corresponding author: derya.balaltuntas@erdogan.edu.tr

ARTICLE IN PRESS

ARTICLE IN PRESS

Abstract

Glioblastoma multiforme represents the most aggressive primary brain malignancy with limited treatment options. Current research critically lacks three-dimensional culture platforms that can both recapitulate native tumor microenvironments and enable quantitative monitoring of cellular behavior. This study presents the first electrochemically-monitored 3D glioblastoma culture system using multi-component PAN nanofiber scaffolds. Six sensor configurations incorporating Ho-MOF, C500, and GO were systematically developed: ITO/PAN, ITO/PAN/MOF, ITO/PAN/C500, ITO/PAN/GO, ITO/PAN/GO/MOF, and ITO/PAN/GO/C500.

Electrochemical impedance spectroscopy unveiled a critical discovery: optimal electrical performance does not guarantee biological compatibility. GO/MOF exhibited lowest electron transfer resistance (31.3 Ω) yet failed completely in cell adhesion. C500-modified scaffolds achieved the important finding 39.8 Ω resistance with >95% cell viability. Cyclic voltammetry delivered current responses (280.53 μA).

Precisely-controlled electrospun nanofibers (392-507 nm diameters, 9-10 μm pores) enabled authentic three-dimensional cellular infiltration. Cytotoxicity testing and Hoechst staining of U-87 MG and LN-18 glioblastoma cells revealed ITO/PAN/C500's dominance: >95% cell viability with organized architecture authentically replicating tumor microenvironment morphology.

This platform obliterates the gap between reductionist 2D models and clinical reality, delivering real-time electrochemical monitoring within physiologically-relevant three-dimensional scaffolds for transformative glioblastoma research applications.

Keywords: Multi-component nanofibers; Glioblastoma cell culture; Three-dimensional scaffolds; Hoechst staining; Cell viability; cytotoxicity testing, Tumor microenvironment

1. Introduction

Cancer research has been significantly constrained by the limitations of traditional two-dimensional (2D) cell culture systems that fail to recapitulate the complex three-dimensional

ARTICLE IN PRESS

(3D) architecture and microenvironmental cues present in native tumors. Glioblastoma multiforme (GBM), classified as a World Health Organization grade IV astrocytoma, represents the most aggressive and prevalent primary brain malignancy, accounting for approximately 45-50% of all primary malignant brain tumors (Ostrom et al., 2021). Despite decades of intensive research and therapeutic development, the median survival for glioblastoma patients remains dismal at 12-15 months, highlighting the urgent need for more effective treatment strategies and improved preclinical models (Tan et al., 2020).

The transition from laboratory research to clinical applications in glioblastoma therapy has been particularly challenging, with numerous promising treatments failing to demonstrate efficacy in human trials despite showing success in conventional 2D culture systems (Verhaak et al., 2010). This disconnect underscores the critical importance of developing more physiologically relevant in vitro models that can better predict therapeutic responses and accelerate the translation of effective treatments to clinical practice.

3D cell culture systems have emerged as a transformative approach to address these limitations by providing a more accurate representation of the native tumor microenvironment (Lv et al., 2017). Unlike conventional 2D cultures, 3D systems facilitate cell-cell and cell-matrix interactions that are crucial for maintaining cellular phenotypes, promoting realistic drug penetration patterns, and enabling the study of complex biological processes such as invasion, angiogenesis, and drug resistance mechanisms (Pampaloni et al., 2007).

ARTICLE IN PRESS

Nanofiber scaffolds fabricated through electrospinning have gained considerable attention in tissue engineering and biomedical applications due to their ability to mimic the natural extracellular matrix (ECM) structure (Agarwal et al., 2008). The electrospinning process enables the production of continuous fibers with diameters ranging from nanometers to micrometers, creating highly porous structures with large surface-to-volume ratios that facilitate cellular adhesion, proliferation, and differentiation (Bhardwaj and Kundu, 2010). PAN has emerged as a particularly promising polymer for nanofiber fabrication due to its excellent mechanical properties, chemical stability, and biocompatibility (Aslan, 2021; Mamuk et al., 2021; Huang et al., 2022; Aslam et al., 2022; Mamuk et al, 2022; Mohite et al., 2023; Mamuk, 2023).

Recent advances in nanofiber technology have focused on incorporating functional additives to enhance scaffold properties and cellular interactions. Coumarin derivatives, known for their

ARTICLE IN PRESS

diverse biological activities and fluorescent properties, have shown potential for improving polymer scaffold characteristics (Leal et al., 2000; Wesseling et al., 2001; Mamuk et al., 2022). Additionally, the integration of conductive substrates such as indium tin oxide (ITO) enables real-time electrochemical monitoring of cellular behavior, providing valuable insights into cell viability, proliferation, and metabolic activity (Soylemez et al., 2016).

Metal-organic frameworks (MOFs) and GO have also garnered attention as nanofiber additives due to their unique properties. Holmium-based MOFs offer interesting optical and magnetic characteristics that can be exploited for biomedical applications (Oylumluoglu et al., 2017). GO, with its excellent mechanical properties and biocompatibility, has been shown to enhance the structural integrity and biological performance of polymer nanofibers (Mohamed et al., 2020).

The development of composite nanofiber systems combining multiple functional components represents a promising strategy for creating advanced 3D culture platforms. However, the optimal composition and fabrication parameters for glioblastoma cell culture applications remain to be established. Furthermore, the integration of electrochemical monitoring capabilities with 3D nanofiber scaffolds presents unique opportunities for developing sophisticated cell analysis platforms.

This study aims to address these challenges by developing and characterizing a novel 3D platform integrating coumarin-enhanced PAN nanofiber scaffolds with ITO electrodes for glioblastoma cell analysis. The research objectives include: (1) optimization of composite nanofiber formulations incorporating coumarin 500, GO, and holmium MOF additives; (2) comprehensive characterization of scaffold morphology, mechanical properties, and thermal behavior; (3) evaluation of glioblastoma cell (U-87 MG and LN-18) viability and morphology on modified scaffolds; and (4) assessment of the platform's potential for 3D cell culture applications.

Several research groups have explored multifunctional scaffold platforms for 3D cancer cell culture. Nanofibrous scaffolds reinforced with graphene oxide (GO) and gelatin, loaded with N-Acetyl cysteine (NAC), have been developed (Yu et al., 2023). Porous scaffolds containing chitosan, gelatin, and graphene oxide have been fabricated for bone tissue engineering [Saravanan et al., 2017).The novelty of this work lies in the systematic integration of multiple functional components within a single scaffold system, specifically designed for glioblastoma

ARTICLE IN PRESS

research applications. The incorporation of coumarin 500 as a bioactive additive, combined with the structural benefits of GO and the unique properties of holmium MOF, creates a multifunctional platform that addresses multiple aspects of 3D cell culture requirements. The integration with ITO electrodes further enhances the platform's analytical capabilities, enabling comprehensive characterization of cellular behavior in a three-dimensional environment.

2. Experimental

2.1. Apparatus

Nanofibers were synthesized using the Inovenso NS1 electrospinning device. The system is a compact setup comprising a programmable syringe pump with a flow-rate accuracy of 0.001 mL h^{-1}, a high-voltage power supply adjustable in the range of 0–40 kV, and a horizontally aligned needle–collector configuration, in which the needle functions as the positive electrode and the target serves as the negative electrode. Structural analysis was performed using Optical Microscopy (OM), Scanning Electron Microscopy (SEM), Thermal Gravimetry (TGA), and Fourier Transform Infrared Spectroscopy (FT-IR) methods. The optical and morphological properties of pure PAN and additive-containing PAN nanofibers were examined using a Zeiss Axio Imager device. For SEM imaging, a JEOL JSM-6510 model scanning electron microscope was used. Thermogravimetric analysis was performed using TGA - TG/DTA 6300 SII EXSTAR6000 equipment capable of measurements in the temperature range of 30-900 °C with a heating rate of 10 °C/minute. DSC measurements were conducted using SII Exstar 6200 model equipment to determine the temperature-dependent phase transition characteristics of nanofibers. In IR spectroscopy, the presence of additives in the nanofiber structure was investigated using FT-IR Device - Perkin Elmer Spectrum 100 equipment.

In cell culture studies, culture controls were performed with a Leica Inverted Microscope (with Fluorescence and CCD Camera). Cytotoxicity analysis of cells was performed using a Thermo Multiskan FC Microplate Reader device. During the preparation of chemical solutions, a Radwag AS 220.R2 Plus analytical balance was used for weighing substances and an Adwa AD8000 model was used for pH adjustment.

ARTICLE IN PRESS

An AUTOLAB-PGSTAT 204 instrument from Metrohm, integrated with NOVA 2.1.4 software, was utilized to carry out cyclic voltammetry (CV) and differential pulse voltammetry (DPV) experiments. The electrochemical setup employed a three-electrode configuration featuring an Ag/AgCl reference electrode (containing 3 M KCl solution), a platinum wire auxiliary electrode (CH Instruments Inc. models CHI111 and CHI115), and a working electrode. Both unmodified and modified PGEs functioned as the working electrodes in these measurements.

2.2. Reagents and Chemicals

In this study, PAN, the version with an average of 150,000 wt (typical) was used (Aslan, 2021; Aslan et al., 2021). Since the PAN molecule consists of strong nitrile groups, it has a polar structure (Figure 1a). This situation increases its interaction with other polar molecules. PAN could be efficiently used as a scaffold for tissue models because it hardens in an amorphous structure after the electrospinning process. In this study, since PAN was to be used as a polymer, 'anhydrous' Dimethylformamide (DMF) from polar solvents was determined as the most suitable solvent. Coumarin 500 (C500) and GO were obtained commercially (Figure 1b-c). Ho-MOF (Figure 1d) was produced by hydrothermal synthesis, which is an environmentally friendly method. 1 mmol $HoCl_3 \cdot 6H_2O$ and 1 mmol 2-sulfoterephthalic acid monosodium salt chemicals were separately dissolved in pure water to form 30 ml aqueous solutions, which were then reacted in a 45 ml teflon container of a steel hydrothermal synthesis reactor through controlled heating and cooling processes at 120°C for 72 hours (Coban et al., 2016; Oylumluoglu et al., 2017). Sigma-Aldrich supplied the following chemicals: potassium dihydrogen phosphate (KH_2PO_4), potassium ferrocyanide ($K_4Fe(CN)_6 \cdot 3H_2O$), potassium hexacyanoferrate ($K_3Fe(CN)_6$), acetylacetone, potassium chloride (KCl), HNO_3 (99.9%), sodium nitrate ($NaNO_3$), sodium hydroxide (NaOH) (98.00%), PAN (Mw ~150,000), and N,N-Dimethylformamide (DMF) (99.80%). Deionized water was utilized for phosphate buffered saline (PBS) preparation. The supporting electrolyte function was served by KCl. For cell culture applications, Dulbecco's phosphate-buffered saline (DPBS) was obtained from Gibco (Thermo Fisher Scientific, Waltham, MA, USA). In vitro cell culture growth supplementation was achieved using heat-inactivated fetal bovine serum (FBS) sourced from Sigma-Aldrich, catalog number F9665.

ARTICLE IN PRESS

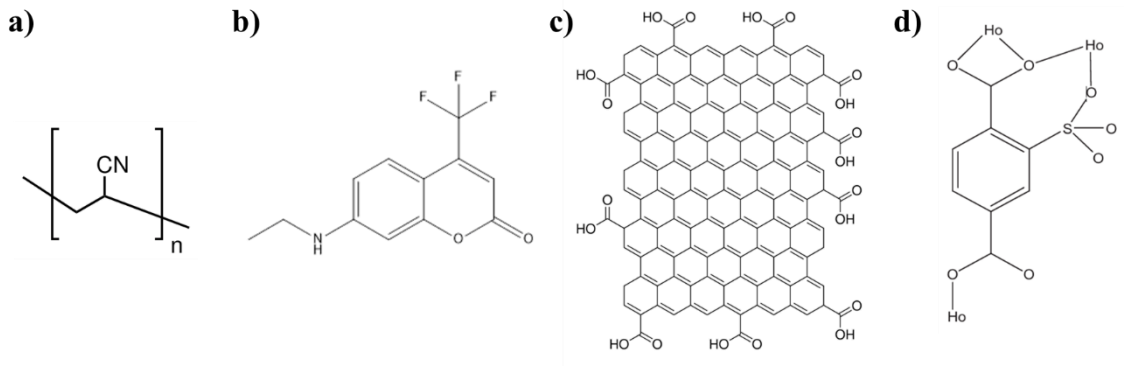

Figure 1. Molecular structures of all substances in the fibers a) Polyacrylonitrile (PAN) (Sigma-Aldrich, n.d.-a) b) Coumarin 500 (C500)) (ChemicalBook, n.d.) c) GO (Sigma-Aldrich, n.d.-b) d) Metal-organic framework (MOF - $C_8H_{11}HoO_{11}S$) (Oylumluoglu et al., 2017)

2.3. Synthesis of Composite Nanofibers by Electrospinning Method

Composite nanofibers were successfully produced with the solutions given in Table 1. Addition of Holmium MOF to PAN, whose production and analysis were reported in previous studies (Coban et al., 2016; Oylumluoglu et al., 2017), was done. GO addition was applied as 1.0 wt% addition with 2.1 MPa Young's modulus (Mohamed et al., 2020). Additionally, 50 ppm C500 addition was made to PAN. All nanofibers were coated onto 1.1×1.1 cm² ITO-coated glasses after undergoing a four-stage cleaning process. A standard deep-green syringe needle with an outer diameter of 0.8 mm and an inner diameter of 0.5 mm was employed throughout all experiments. The collector consisted of a metal target covered with a 20 µm-thick aluminum foil, onto which glass substrates were mounted. Throughout the entire fiber coating process, the environmental temperature was determined to be 23±1°C and relative humidity was %35±%3. Composite nanofibers were produced by electrospinning method using the prepared precursor solutions (Figure 2). In the electrospinning process, all nanofibers were produced with electrospinning parameters of 15 kV – 23 cm – 0.6 ml/h.

ARTICLE IN PRESS

Table 1. List of Solution Concentrations

Code	Solution	Content Solution	Concentration
TP001	PAN	DMF	
		PAN	%9,0
TP002	PAN/Ho-MOF	DMF	
		PAN	%9,0
		Ho- MOF	%0,03

ARTICLE IN PRESS

TP003	PAN/C500	DMF	
		PAN	%9,0
		C500	1,0 ppm
TP004	PAN/GO	DMF	
		PAN	%9,0
		GO	%1,0
TP005	PAN/GO/Ho-MOF	DMF	
		PAN	%9,0
		GO	%1,0
		Ho-MOF	%0,03
TP006	PAN/GO/C500	DMF	
		PAN	%9,0
		GO	%1,0
		C500	1,0 ppm

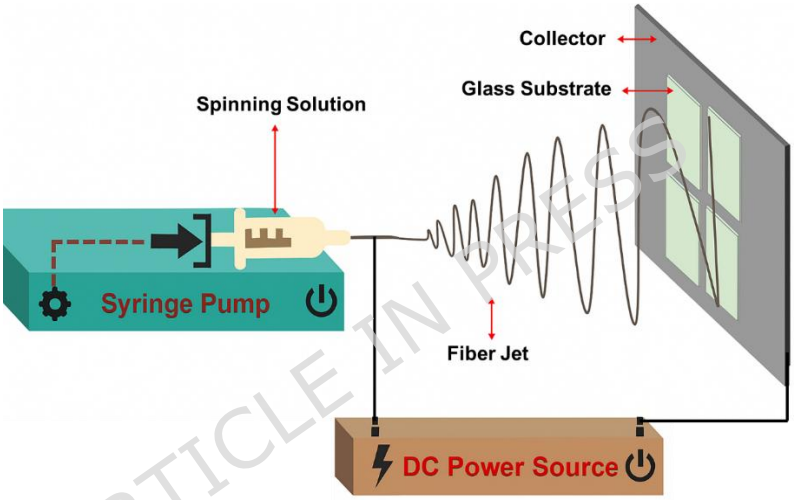

Figure 2. Schematic representation of the electrospinning process.

Precursor solutions were calculated and prepared using the calculation technique given in Equations 2.1, 2.2, 2.3, and 2.4. The basic precursor solution DMF/PAN solution was prepared using Equation 2.1, and additive solutions using GO, Ho-MOF, and C500 as additive materials were prepared using Equations 2.2, 2.3, and 2.4, respectively. In the electrospinning process, all nanofibers were produced with electrospinning parameters of 15.0 kV – 23.0 cm – 0.6 - 0.7 ml/h.

$$\%\ \text{concentration (by weight)} = \frac{\text{solute (g)}}{\text{solute (g)} + \text{solvent (g)}} \quad \textbf{(1)}$$

$$\%\ \text{concentration (by weight)} = \frac{\text{additive (GO) (g)}}{\text{additive (GO) (g)} + \text{PAN (g)}} \quad \textbf{(2)}$$

ARTICLE IN PRESS

$$\%\ \text{concentration (by weight)} = \frac{\text{additive (Ho–MOF,C500) (g)}}{\text{additive (Ho–MOF,C500) (g) + (PAN + GO) (g)}} \quad \textbf{(3)}$$

$$ppm = \frac{\text{additive (C500) (µg))}}{\text{total volume (mL)}} \quad \textbf{(4)}$$

2.4. Cell Culturing

In the study, human glioblastoma-like cell line U-87 MG and Grade IV brain tumor cells from laboratory stocks were used. The glioblastoma cell line LN-18 was obtained from the American Type Culture Collection (ATCC). The U-87 MG cell line was kindly provided by Prof. Sevgi Irtegun Kandemir (Dicle University, Diyarbakır, Türkiye). U-87 MG and LN-18 cells were cultured in high glucose DMEM medium, and ARPE-19 normal retinal epithelial cells were cultured in RPMI medium supplemented with 10% Fetal Bovine Serum (FBS) (Sigma-Aldrich) and 1% Penicillin/Streptomycin, at 37°C in a cell culture incubator with 5% CO_2. All solutions used in the culture process were sterilized with 0.22 µm filters before use. Cells were grown in 75 cm^2 sterile flasks to reach sufficient cell numbers for experiments. Depending on the experimental purpose, sterile 6, 24, or 96-well plates or 9 cm petri dishes were used. For cell passaging and preparation for experiments, after removing the medium, cells were washed with sterile dPBS solution and removed from culture vessels using Trypsin/EDTA solution. Cell counting was performed using the trypan blue staining method to determine cell numbers for experiments. All cell culture procedures were performed under laminar flow and sterile conditions. PAN-coated and modified coverslips were kept in 70% ethanol for 20 minutes, then ethanol was removed. Subsequently, they were treated with PBS twice for 15 minutes each. After removing PBS, cell seeding procedures continued. U-87 MG and LN-18 cells were seeded at a density of 1.25×10^5 cells/well onto sterile modified 3D PAN nanofiber scaffold-coated coverslips placed in 12-well plates. Cells were cultured at 37°C in a cell culture incubator with 5% CO_2.

2.5. Cell Viability Assay

Cell viability and proliferation on the modified PAN nanofiber scaffolds (5x5mm) were assessed using the Cell Counting Kit-8 (CCK-8) assay. Cells were cultured on the scaffolds in 96-well plates for 7 days. On the day of analysis, CCK-8 reagent was added to the wells, and cells were incubated for 1 hour at 37 °C with 5% CO_2. Subsequently, supernatants were

ARTICLE IN PRESS

transferred to a new 96-well plate and absorbance was measured using a microplate reader to quantify metabolic activity as an indicator of cell viability.

3. Results

3.1. Electrochemical Studies

During the modification of bare ITO glass electrodes and fabrication stage of the cytosensor, pure PAN and composite additive-containing PAN nanofibers were synthesized on ITO glass electrodes. The electrodes were characterized electrochemically. To create a 3D optimal environment, modified ITO electrodes were modified with ECM elements (fibronectin or collagen IV).

3.1.1. Modification of Bare ITO Electrode and Cytosensor Formation

During the modification of bare ITO glass electrodes and fabrication stage of the cytosensor, pure PAN and composite additive-containing PAN nanofibers were synthesized onto ITO glass electrodes. For the formation of 3D optimal environment, modified ITO electrodes were modified with ECM elements (fibronectin or collagen IV). For the formation of the glioblastoma tumor model, cell lines (U-87 MG or LN-18) were cultured on ECM-incorporated modified ITO electrodes to achieve cytosensor fabrication. Separate quantity optimizations were performed for fibronectin (FN) and collagen IV (COL IV) used by DPV method. Changes in ECM additive material-containing modified ITO electrodes after cell modification were determined at cellular level and with electrochemical characterization.

ARTICLE IN PRESS

3.1.2. Establishment of Working Range

Before cell modification, all electrochemical measurements were performed within the three-electrode system by attaching the composite nanofiber-coated ITO electrodes and bare ITO working electrode listed in Table 2 to the connector with crocodile clips.

ARTICLE IN PRESS

Table 2. Composite Nanofiber-Coated ITO Working Electrodes

Electrode nomenclature	TP001	TP002	TP003	TP004	TP005	TP006
Electrode modification	ITO/PAN	ITO/PAN/ MOF	ITO/PAN/ C500	ITO/PAN/ GO	ITO/PAN/GO/ MOF	ITO/PAN/GO/C 500

3.1.3. Determination of Optimal Electrode Combination

Cell adhesion and growth performances were examined in PAN nanofibers produced with specified optimal amounts of FN and COL(IV) additives for U-87 MG and LN-18 cells. At the same time, electrochemical responses of electrodes containing additive materials in these amounts were measured by DPV and EIS methods. Subsequently, the electrode combination that gave the best response was determined (ITO/PAN/X/Cell) and optimizations were made for this electrode.

3.1.4. *Other Optimizations for Optimal Electrode Combination*

After microscopic and electrochemical characterization of the optimal electrode combination ITO/PAN/C500/COL 10µg/ml determined for U-87 MG cell line, optimization of working conditions was performed. The optimal temperature at which cells created the best electrochemical response for ITO/PAN/C500/COL 10µg/ml electrode was investigated by DPV method. After determining the optimal temperature, the incubation time for modification of ITO/PAN/C500/COL 10µg/ml electrode with U-87 MG cell was investigated. The analytical characteristics of the ITO/PAN/C500/COL 10µg/ml/U-87 MG cytosensor developed under optimal working conditions were determined. A calibration graph was created for the cytosensor cultured with different numbers of cells, and LOD (3s/m) and LOQ (10s/m) values were determined. Measurements obtained from the median measurement in the calibration graph enabled the determination of the repeatability performance of the electrodes. These measurements were made with at least 5 repetitions and RSD value was calculated.

The same procedure was applied for ITO/PAN/C500/FN 1µg/ml, which is the optimal electrode combination determined for LN-18 cell line. Temperature, incubation, and analytical characteristics were determined.

Composite nanofibers were successfully produced with the solutions given in Table 2. GO addition was applied as 1.0 wt% addition with 2.1 MPa Young's modulus (Mohamed et al.,

ARTICLE IN PRESS

2020). PAN nanofibers with 0.01%, 0.03%, 0.1%, 0.3%, and 1.0% Ho-MOF additives were produced and the optimal concentration was determined to be 0.03% by Cyclic Voltammetry (CV) and Differential Pulse Voltammetry (DPV) measurements in Figure 3.

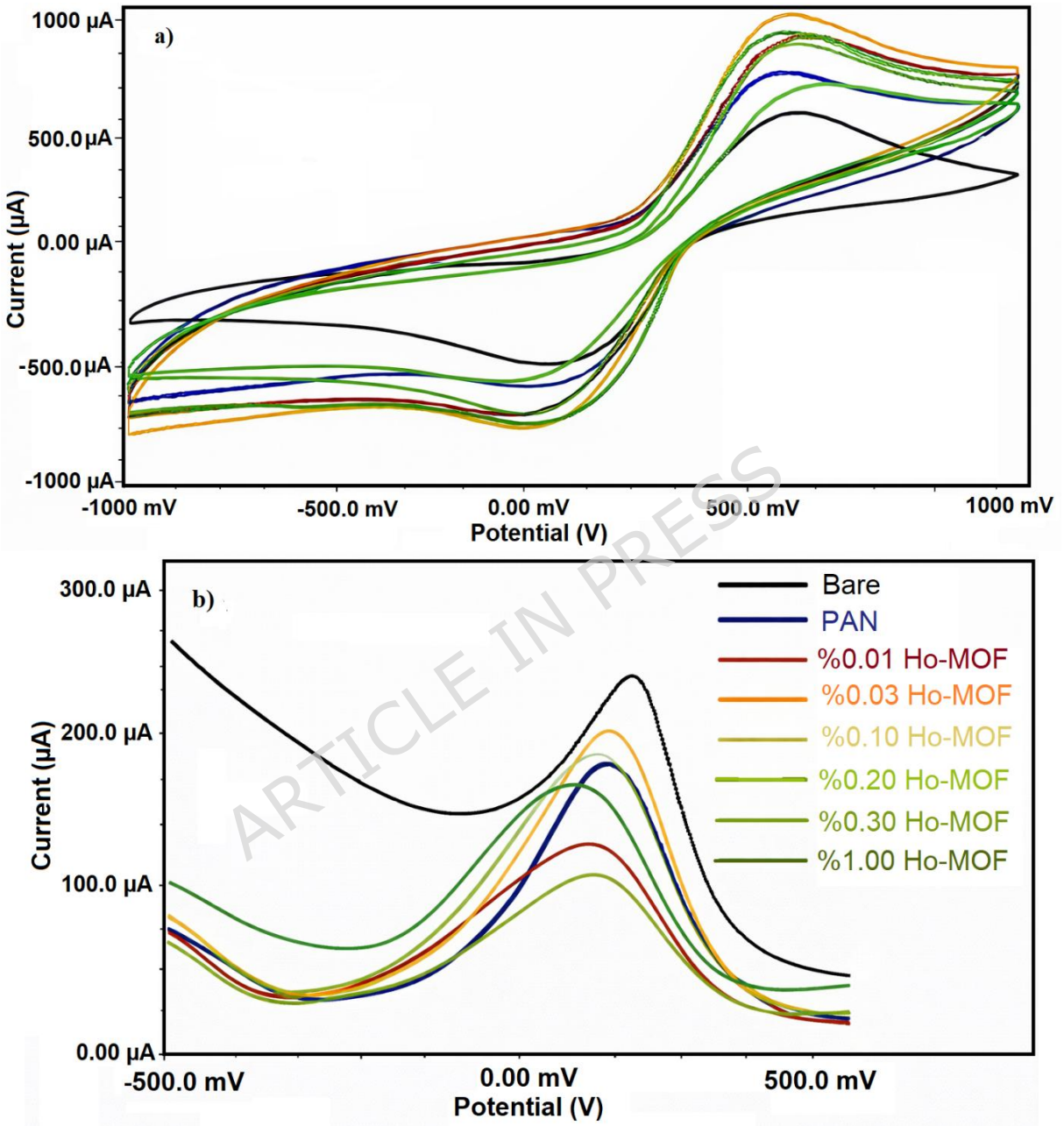

Figure 3. a) CV and b) DPV measurement results of Ho-MOF incorporated PGE-PAN electrodes.

For optimizations of Ho-MOF, GO, C500 incorporated PGE-PAN electrodes, CV measurements were determined in 50 mM PBS (pH 7.4) containing 5mM $[Fe(CN)_6]^{3-/4-}$ with

ARTICLE IN PRESS

working range -1 V to +1 V, scan rate: 100 mV/s. In DPV measurements, working range was -500 to +500 mV scan rate: 50 mV/s.

When CV measurements are examined, the widest region is scanned by the 0.03% Ho-MOF added electrode. DPV measurements also show that the 0.03% Ho-MOF added electrode gives the highest response, results for each electrode are given in Table 3. Figure 4 shows the DPV results of Ho-MOF incorporated PGE-PAN electrodes in column graph form with standard deviations.

The 0.03% Ho-MOF added electrode gave the highest current response with 217 µA peak response. This value is almost as high as the bare electrode; the bare electrode gave a current value of 254 µA and this electrode's current is 14.57% lower than the bare one. However, the current of the 0.03% Ho-MOF added electrode is 14.21% higher than the current of the PAN-coated electrode showing 190 µA current value.

Table 3. DPV Results of Ho-MOF Incorporated PGE-PAN Electrodes

Electrode	DPV current (µA)	Current difference with bare electrode (%)	Current difference with PAN-coated electrode (%)
Bare	254.00	-	33.68
PAN coated	190.00	-25.20	0.00
%0,01 Ho-MOF	130.00	-48.82	-31.58
%0,03 Ho-MOF	217.00	-14.57	14.21
%0,10 Ho-MOF	194.00	-23.62	2.11
%0,30 Ho-MOF	105.00	-58.66	-44.74
%1,00 Ho-MOF	176.00	-30.71	-7.37

ARTICLE IN PRESS

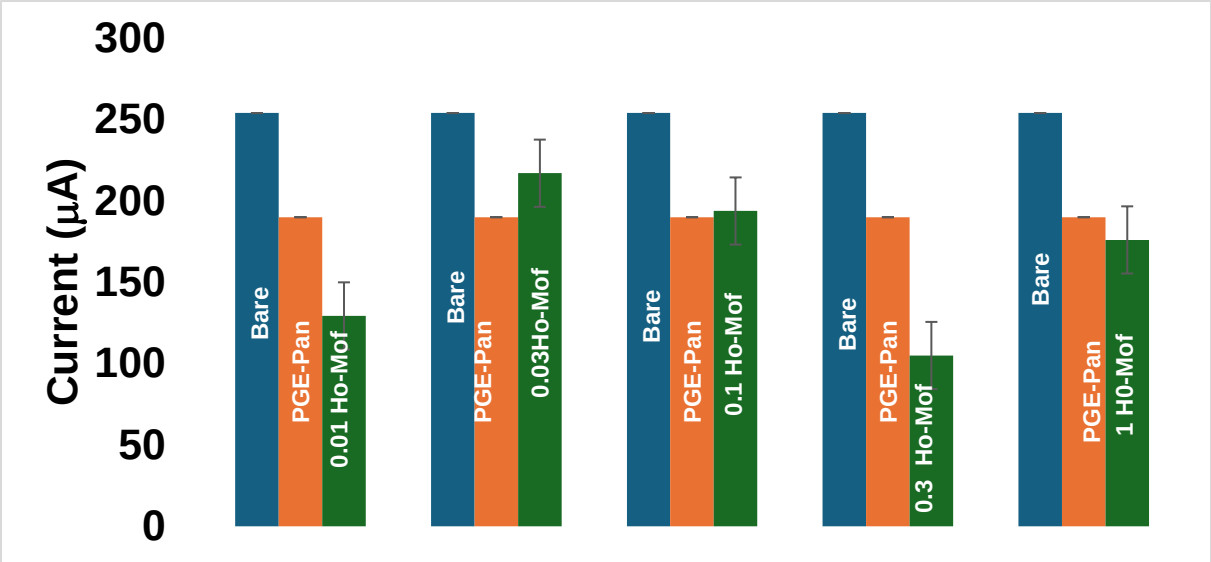

Figure 4. Column graph representation of DPV results of Ho-MOF incorporated PGE-PAN electrodes.

PAN nanofibers with 0.1%, 0.3%, 1%, 3%, and 10% GO additives were produced and the optimal concentration was determined to be 1% by Cyclic Voltammetry (CV) and Differential Pulse Voltammetry (DPV) measurements. Experimental results are given with graphs in Figure 5.

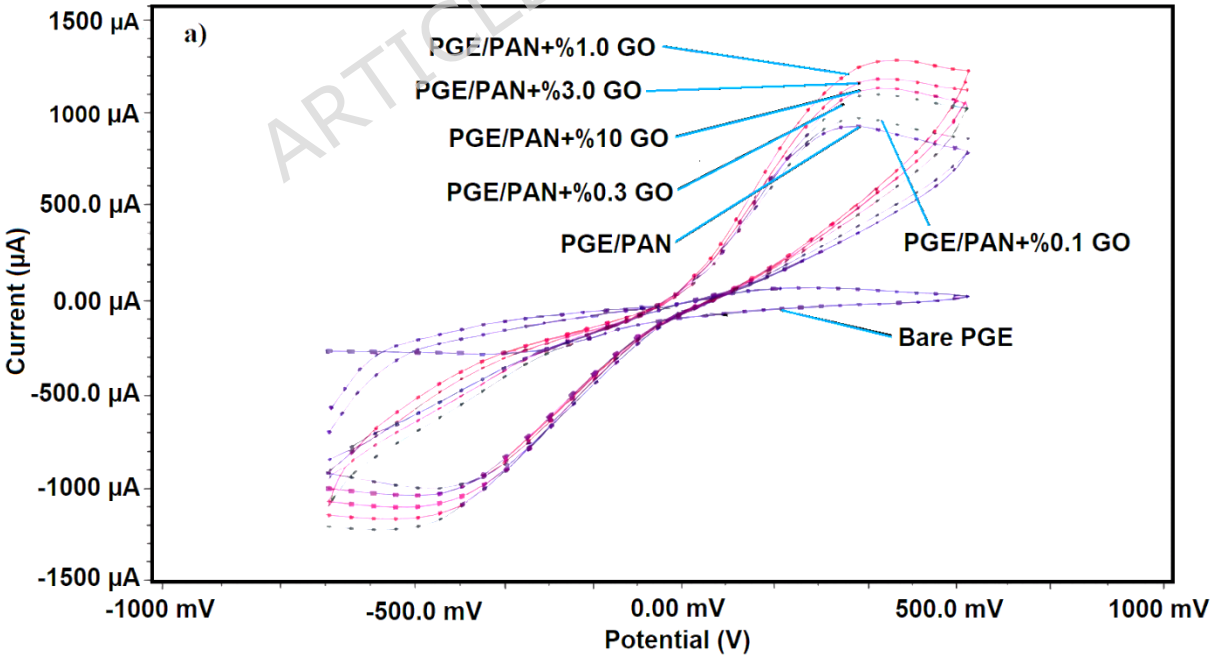

ARTICLE IN PRESS

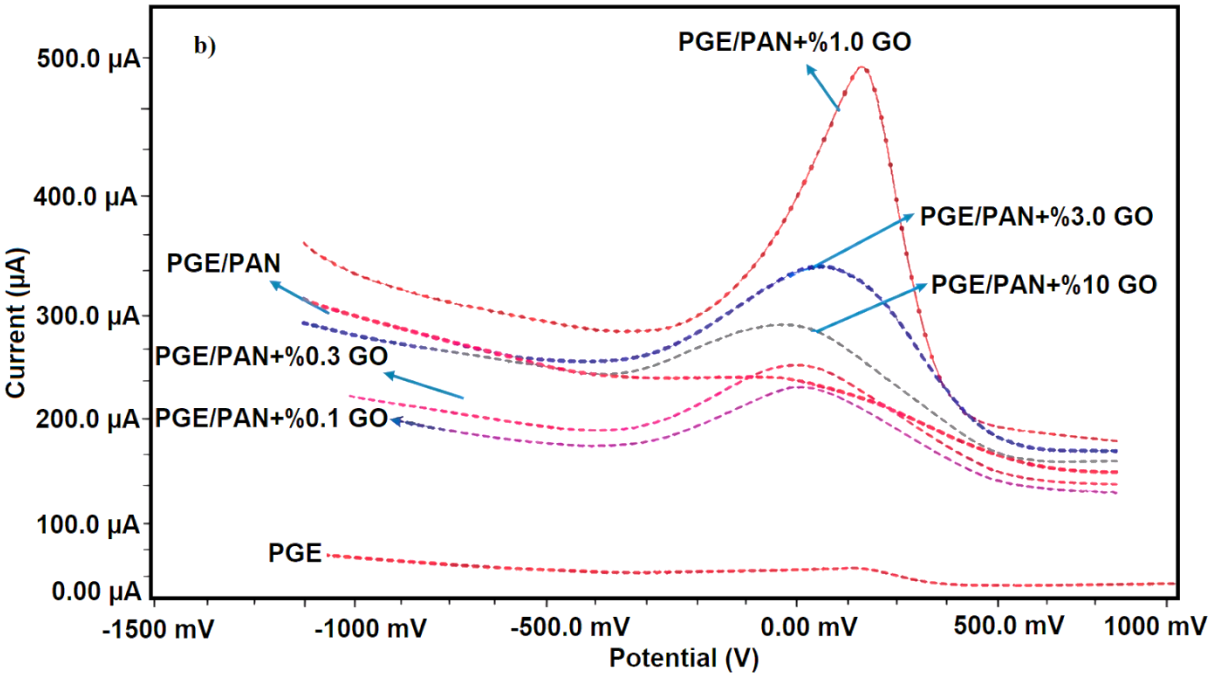

Figure 5. a) CV and b) DPV measurement results of GO incorporated PGE-PAN electrodes.

When CV measurements are examined, the widest region is scanned by the 1% GO added electrode. DPV measurements also show that the 1% GO added electrode gives the highest response, results for each electrode are given in Table 4. The 1% GO added electrode gave the highest current response with 222.5 µA peak response. Figure 6 shows the DPV results of GO incorporated PGE-PAN electrodes in column graph form with standard deviations.

Table 4. DPV Results of GO Incorporated PGE-PAN Electrodes

Electrode	DPV current (µA)	Difference with bare electrode (%)	Difference with PAN-coated electrode (%)
Bare PGE	66.11	-	-61.83
PGE/PAN	173.20	161.99	0.00
%0.1 GO	194.60	194.36	12.36
%0.3 GO	206.80	212.81	19.40
%1 GO	222.50	236.56	28.46
%3 GO	196.20	196.78	13.28
%10 GO	190.20	187.70	9.82

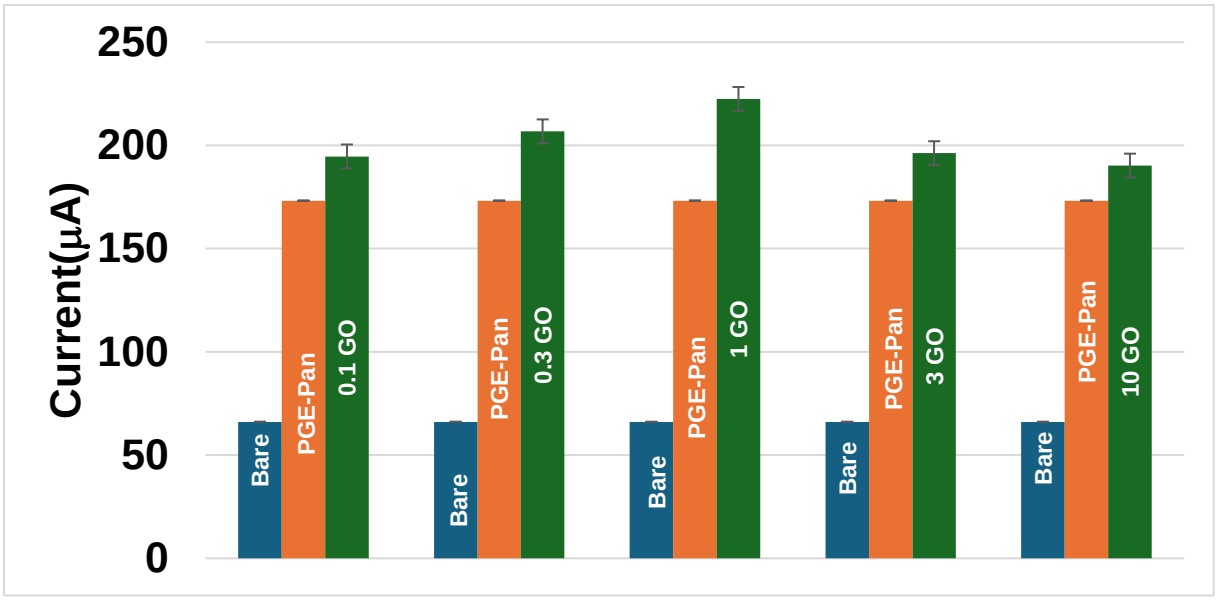

Figure 6. Column graph representation of DPV results of GO incorporated PGE-PAN electrodes.

PAN nanofibers with 10%, 20%, 50%, 100%, 200% C500 additives were produced and the optimal concentration was determined to be 50% by Cyclic Voltammetry (CV) and Differential Pulse Voltammetry (DPV) measurements. Experimental results are given with graphs in Figure 7.

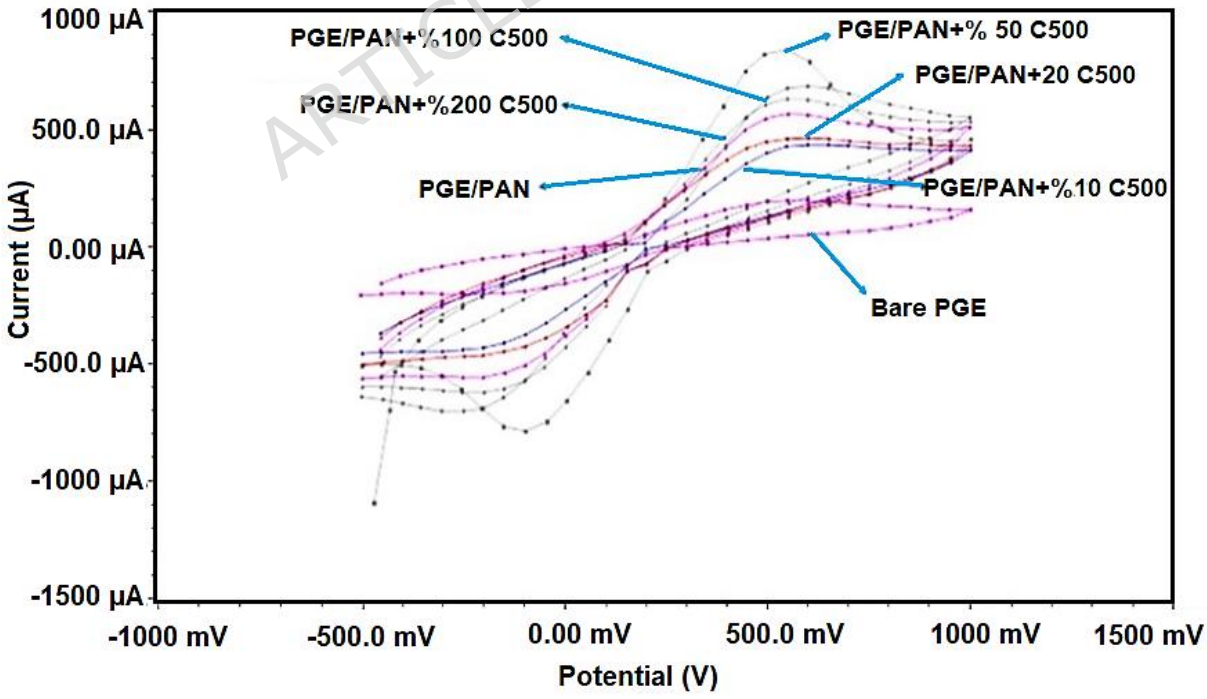

Figure 7. CV measurement results of C500 incorporated PGE-PAN electrodes.

ARTICLE IN PRESS

When CV measurements are examined, the widest region is scanned by the 50% C500 added electrode. DPV measurements also show that the 50% C500 added electrode gives the highest response, results for each electrode are given in Table 5. The 50% C500 added electrode gave the highest current response with 280.53 µA peak response. Figure 8 shows the DPV results of C500 incorporated PGE-PAN electrodes in column graph form with standard deviations.

All nanofibers were grown on 1.1×1.1 cm² ITO-coated glasses that underwent a four-stage cleaning process. Throughout the entire fiber growth process, the environmental temperature was determined to be 23±1°C and relative humidity was 35±3%. Composite nanofibers were produced by electrospinning method using the prepared MET solutions.

Table 5. DPV Measurement Results of C500 Incorporated PGE-PAN Electrodes

Electrode	DPV current (µA)	Difference with bare electrode (%)	Difference with PAN-coated electrode (%)
Bare PGE	63.09	-	-28.14
PGE/PAN	87.79	39.15	-
%10 C500	124.77	97.77	42.12
%20 C500	128.97	104.42	46.91
%50 C500	280.53	344.65	219.55
%100 C500	158.10	150.59	80.09
%200 C500	152.50	141.72	73.71

ARTICLE IN PRESS

ARTICLE IN PRESS

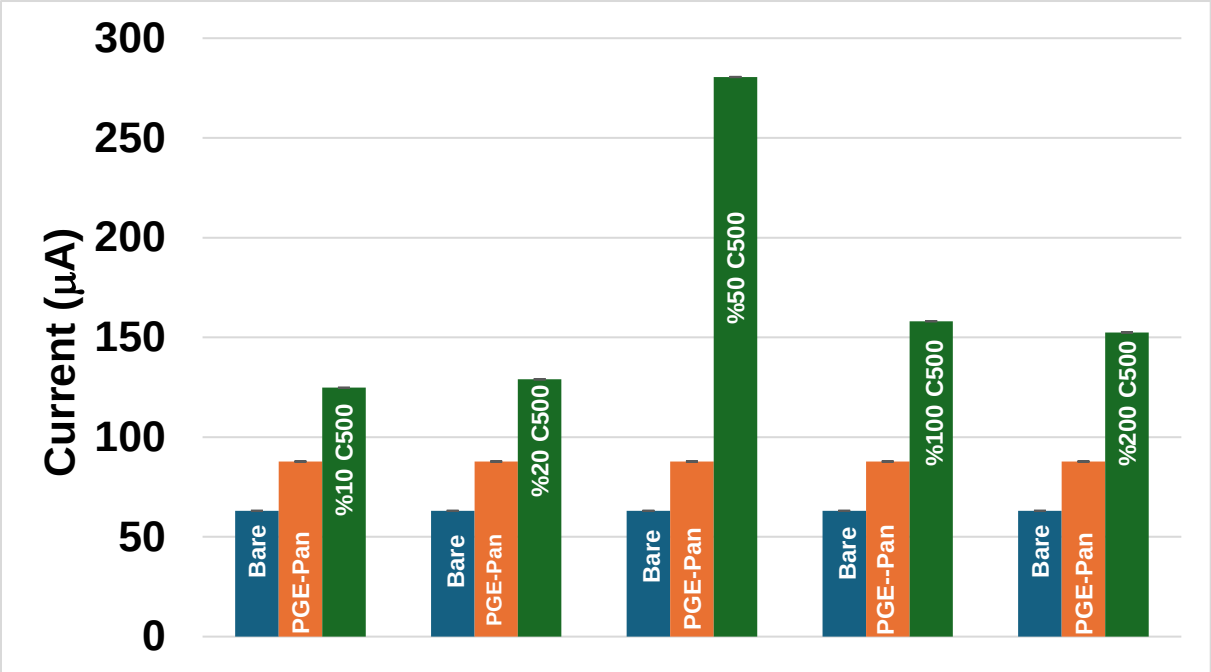

Figure 8. Column graph representation of DPV results of C500 incorporated PGE-PAN electrodes

Electrochemical Impedance Spectroscopy (EIS) Analysis

EIS analysis was performed to evaluate the electrochemical properties of all modified electrodes before and after cell modification. The equivalent circuit model $[Rs(RQ)_1(RQ)_2]$ was fitted to the experimental data with excellent correlation (x^2 values ranging from 0.000425 to 0.039518). Table 6 presents the charge transfer resistance (Rct) values and fitting parameters for all electrode configurations.

Table 6 . Circuit Elements Table

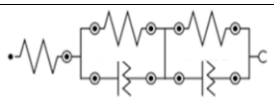	**Circuit**	**R_{ct}:** Charge transfer resistance	**X^2** chi-squared
ITO	$[R_s(RQ)_1(RQ)_2]$	853 Ω	0.011294
ITO/PAN	$[R_s(RQ)_1(RQ)_2]$	115 Ω	0.018628
ITO/PAN/C500	$[R_s(RQ)_1(RQ)_2]$	39.8 Ω	0.002199
ITO/PAN/GO/MOF	$[R_s(RQ)_1(RQ)_2]$	31.3 Ω	0.000684
ITO/PAN/MOF	$[R_s(RQ)_1(RQ)_2]$	79.8 Ω	0.039518
ITO/PAN/GO	$[R_s(RQ)_1(RQ)_2]$	50.6 Ω	0.001355
ITO/PAN/GO/C500	$[R_s(RQ)_1(RQ)_2]$	36.9 Ω	0.000425
ITO/PAN/LN-18	$[R_s(RQ)_1(RQ)_2]$	839 Ω	0.01

ARTICLE IN PRESS

ITO/PAN/C500/ LN-18	$[R_s(RQ)_1(RQ)_2]$	1.47 kΩ	0.04
ITO/PAN/GO/MOF/LN-18	$[R_s(RQ)_1(RQ)_2]$	52.9 Ω	0.001
ITO/PAN/MOF/LN-18	$[R_s(RQ)_1(RQ)_2]$	58.2 Ω	0.004
ITO/PAN/GO/LN-18	$[R_s(RQ)_1(RQ)_2]$	55.1 Ω	0.002
ITO/PAN/GO/C500/LN-18	$[R_s(RQ)_1(RQ)_2]$	147 Ω	0.002
ITO/PAN/U87-MG	$[R_s(RQ)_1(RQ)_2]$	126 Ω	0.006
ITO/PAN/C500/U87-MG	$[R_s(RQ)_1(RQ)_2]$	1.34kΩ	0.003
ITO/PAN/GO/MOF/U87-MG	$[R_s(RQ)_1(RQ)_2]$	48.6 Ω	0.001
ITO/PAN/MOF/U87-MG	$[R_s(RQ)_1(RQ)_2]$	1.10kΩ	0.03
ITO/PAN/GO/U87-MG	$[R_s(RQ)_1(RQ)_2]$	65.7Ω	0.001
ITO/PAN/GO/C500/U87-MG	$[R_s(RQ)_1(RQ)_2]$	71.4Ω	0.005

In Table, the circuit for the modified electrodes in table 6. The equivalent circuit model $[Rs(RQ)_1(RQ)_2]$ was fitted to the experimental data with excellent correlation, as evidenced by low chi-squared (χ^2) values ranging from 0.000425 to 0.039518. These low χ^2 values confirm the high quality of the fitting and reliability of the equivalent circuit model for all electrode configurations.

ITO , ITO/PAN, ITO/PAN/GO/C500, ITO/PAN/GO/MOF, ITO/PAN/MOF, ITO/PAN/GO, ITO/PAN/C500 was determined as $[Rs(RQ)_1(RQ)_2]$ with minimum estimated errors of 0.011294%, 0.018628%, 0.002199%, 0.000684%, 0.039518%, 0.001355%, and 0.000425%, respectively. Following cell modification, notable changes in transfer resistance were observed, reflecting the impact of cell-electrode interface interactions on electrochemical properties. LN-18 cells caused more significant resistance increases compared to U-87 MG cells, particularly evident in C500-modified electrodes where resistance increased from 39.8 Ω to 1.47 kΩ for LN-18 versus 1.34 kΩ for U-87 MG cells.

The results revealed significant variations in electron transfer resistance across different modifications. Bare ITO electrode exhibited high transfer resistance (853 Ω), which decreased substantially to 115 Ω upon PAN coating. Among the additive-containing electrodes, GO/MOF combination showed the lowest transfer resistance (31.3 Ω), followed by GO/C500 (36.9 Ω) and C500 alone (39.8 Ω).

Importantly, while GO/MOF combination demonstrated superior electrochemical properties, this configuration failed to support cell adhesion in subsequent biological assays. This finding highlights the critical importance of balancing electrochemical performance with biocompatibility in developing cell

ARTICLE IN PRESS

culture platforms. The C500-modified electrode achieved optimal balance, providing low transfer resistance while maintaining excellent cell viability and proliferation.

Following cell modification, notable changes in transfer resistance were observed, reflecting the impact of cell-electrode interface interactions on electrochemical properties. These variations provide valuable insights into the dynamic nature of the bioelectrochemical interface during cell culture.

Cyclic Voltammetry Characterization

Cyclic voltammetry analysis provided complementary insights into the redox behavior and electron transfer kinetics of the modified electrodes. Table 7 summarizes the anodic (Ea) and cathodic (Ec) peak potentials, corresponding current values (Ia, Ic), and peak separation (ΔE) for all electrode configurations.

In Table the current and ΔE values obtained from the CV curves of all combinations .

Table 7. Current and ΔE values obtained from CV curves

Sensors	Ea (V)	Ia (μA)	Ec (V)	Ic (μA)	ΔE (V)
ITO	0.42023	455.12	0.068665	357.55	0.351565
ITO/PAN	0.41046	956.52	0.09552	862.53	0.31494
ITO/PAN/MOF	0.39093	951.62	0.11505	887.86	0.27588
ITO/PAN/C500	0.42023	1125.1	0.083313	1049.2	0.336917
ITO/PAN/GO	0.42267	817.77	0.085754	898.85	0.336916
ITO/PAN/GO/MOF	0.4007	1155	0.11017	1107	0.29053
ITO/PAN/GO/C500	0.38361	1168.6	0.11261	1097.9	0.271

ARTICLE IN PRESS

The analysis revealed that electrode modifications significantly influenced both peak currents and electrochemical reversibility. Bare ITO electrode showed moderate current responses (455.12 μA anodic, 357.55 μA cathodic) with a peak separation of 0.352 V. PAN coating enhanced current responses substantially (956.52 μA anodic, 862.53 μA cathodic) while improving electrochemical reversibility (ΔE: 0.315 V).

The highest current responses were achieved with GO/C500 combination (1168.6 μA anodic, 1097.9 μA cathodic), which also exhibited the best electrochemical reversibility (ΔE: 0.271 V). This

ARTICLE IN PRESS

configuration demonstrated the synergistic effect of GO and coumarin 500 in enhancing electron transfer kinetics. C500 modification alone also showed excellent performance (1125.1 μA anodic, 1049.2 μA cathodic), confirming its effectiveness as a bioactive additive.

These electrochemical characterization results, combined with EIS analysis, provided crucial guidance for optimizing electrode configurations for subsequent cell culture applications. The correlation between electrochemical performance and biological compatibility established the foundation for developing effective 3D glioblastoma culture platforms. DPV measurements were determined in 50 mM PBS (pH 7.4) containing 5mM $[Fe(CN)_6]^{3-/4-}$ with working range -0.3V to +0.6 V, scan rate: 50 mV/s. For CV measurements, the working range was determined as -0.3 to +0.8 V in 50 mM PBS (pH 7.4) PBS buffer solution containing 5mM $[Fe(CN)_6]^{3-/4-}$, scan rate: 100 mV/s. Electrochemical characterizations of the electrodes given in Table 2 after cell modification were performed by DPV and EIS methods. Additionally, composite PAN nanofibers incorporated with FN and COL (IV) for providing 3D optimal environment were also electrochemically characterized.

Lower ΔE values indicate better electrochemical reversibility and faster electron transfer kinetics, which are crucial for sensitive real-time monitoring applications. The excellent reversibility observed in GO/C500 configuration (ΔE: 0.271 V) demonstrates optimal electron transfer characteristics for biosensing applications.

ARTICLE IN PRESS

3.3. Structural Analysis

Optical analyses were first performed to observe whether the nanofibers were produced uniformly. Optical imaging of the fibers was performed in transmission mode. First, to check whether there was anisotropic property in the fibers spun on the microscope slide, samples were placed between the cross-positioned polarizers of the polarized optical microscope (POM). If a material does not prevent the incoming light from reaching the eyepieces when positioned between cross polarizers, these materials are anisotropic and have the ability to change the polarization direction of polarized light. As is known, the birefringence of the PAN polymer used as the host material in fibers is quite low (0.01 at 23°C) (An et al, 2006), meaning it is not expected to give an image (brightness) in POM. If other materials added to PAN are anisotropic, texture (pattern) can be obtained in POM images. However, no texture was detected for all fiber samples between cross polarizers and only a dark (completely black) image was obtained. This situation indicates that the fibers do not have any anisotropy. Upon this, polarizers were disabled and optical microscope (OM) images were taken. 40x magnification was applied to obtain textures in transmission mode. Figure 9 contains textures of the spun fibers. When Figure

ARTICLE IN PRESS

9 is examined, it is seen that each sample is spun uniformly. There are no bead structures along the fibers.

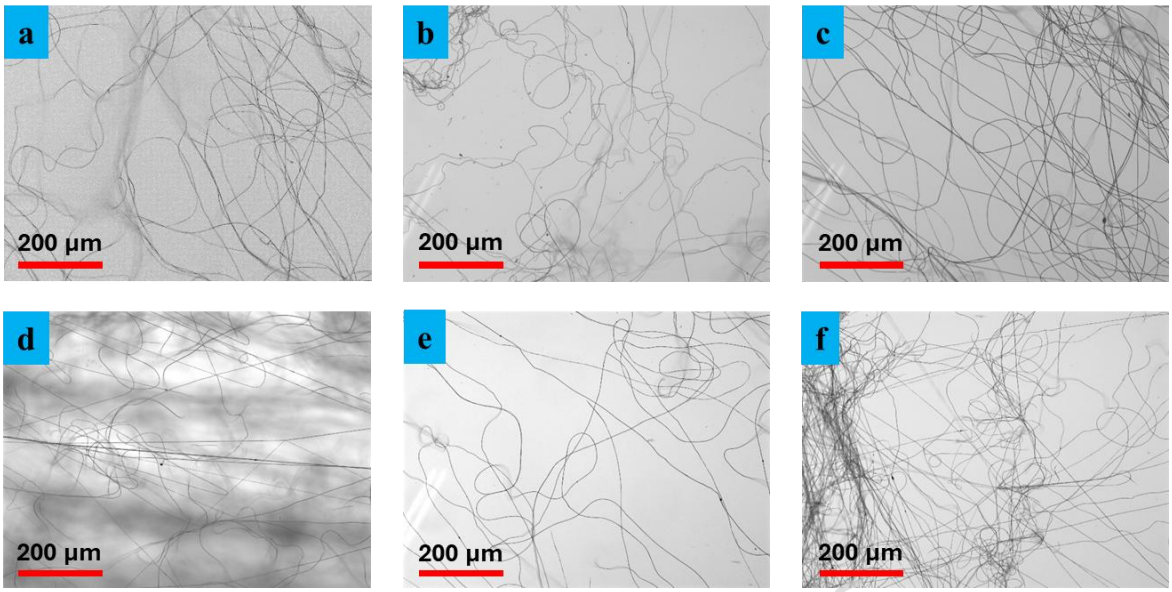

Figure 9. OM images of PAN fibers. (a) ITO/PAN, (b) ITO/PAN/MOF, (c) ITO/PAN/C500, (d) ITO/PAN/GO, (e) ITO/PAN/GO/MOF, (f) ITO/PAN/GO/C500. SCALE represents 200 µm length.

Structural analyses of nanofibers were performed through SEM images. Since all samples were grown on glass and PAN is an insulating material, they were coated with a gold layer for 60 seconds under argon inert gas before SEM observation to eliminate the charging effect and obtain higher quality images.

Figure 10 presents the SEM micrographs and corresponding fiber diameter distributions of nanofibers deposited on composite nanofiber-coated ITO working electrodes (Table 2). Determining the distribution of fiber thicknesses from SEM images was performed using the Fiji application (Schindelin et al., 2012). According to the scaling function of the Fiji application, the length scale of a SEM image corresponds to 100 pixels. A two-pixel error between the starting and the ending points during the determination of the thickness of any fiber indicates that an error of ±10 nm in measurements is acceptable. Overall, all samples exhibit continuous and predominantly uniform fiber morphologies, with diameter distributions centered in the submicron range. As shown in Figure 10a, the fibers display generally uniform extension. Minor bead-like features are observed locally; however, these structures are elongated along the fiber axis rather than spherical. Fiber diameters range from approximately

ARTICLE IN PRESS

325 to 625 nm, with a strong concentration between 400 and 525 nm, yielding an average diameter of 453 nm. For the PAN/C500 sample (Figure 10b), fiber diameters vary between 400 and 625 nm. Although complete uniformity is not achieved, the distribution spans a relatively wide range, as reflected by the broader Gaussian profile. Most fibers fall within the 400–525 nm interval, and this sample exhibits the highest average fiber diameter (507 nm). The PAN/GO fibers (Figure 10c) appear morphologically uniform, however, irregularly shaped particles attached to the fiber surfaces are clearly visible and attributed to GO incorporation. Despite the broad diameter range (300–650 nm), a highly uniform distribution is achieved, with most fibers concentrated between 400 and 500 nm. The average fiber diameter is 451 nm. In the PAN/MOF sample (Figure 10d), fibers predominantly extend along a common direction and show a uniform morphology. Occasionally elongated and swollen nonuniformities are observed in the background. Fiber diameters range from 300 to 525 nm, with most fibers distributed between 350 and 430 nm, resulting in the lowest average fiber diameter of 392 nm. The PAN/GO/C500 fibers (Figure 10e) exhibit a highly uniform morphology without visible structural defects. Similar to PAN/GO fibers, surface irregularities attributed to GO particles are observed. Although this sample shows the widest diameter range (275–625 nm), the majority of fibers are narrowly distributed between 350 and 475 nm, with an average fiber diameter of 402 nm. Finally, Figure 10f shows that the PAN/GO/MOF fibers are uniformly spun, with diameters distributed between 300 and 650 nm. Most fibers fall within the 400–525 nm range, and the average fiber diameter is calculated as 462 nm.

ARTICLE IN PRESS

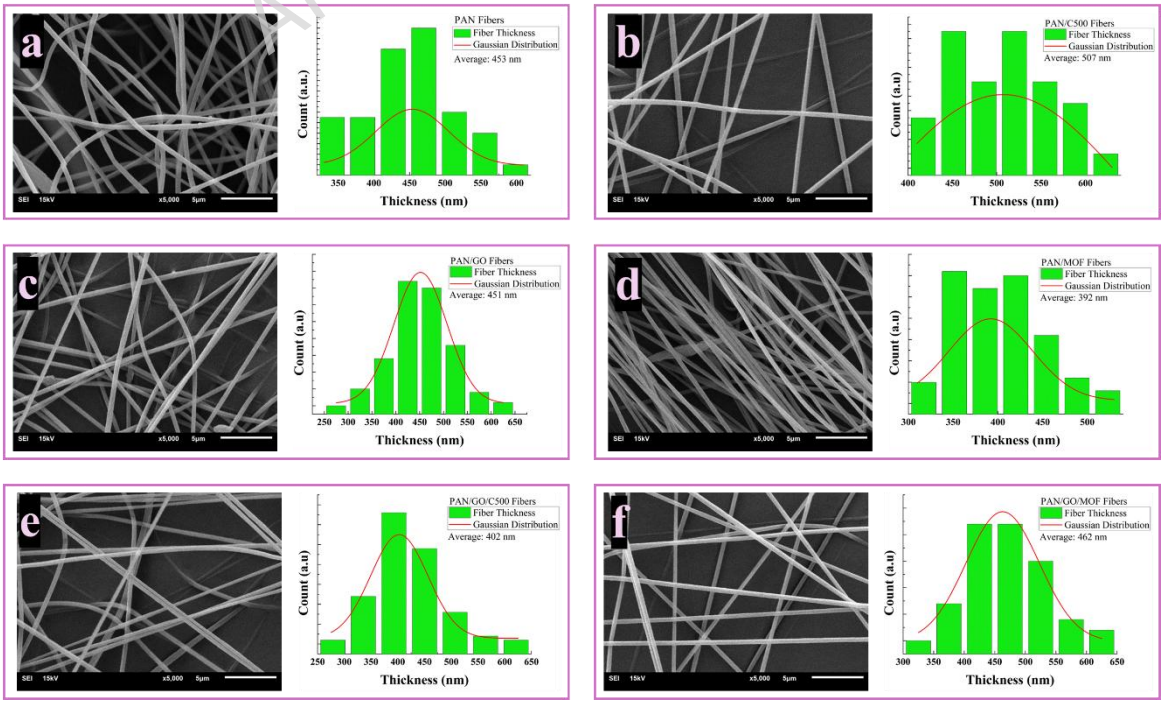

ARTICLE IN PRESS

Figure 10. a) PAN b) PAN/C500 c) PAN/GO d) PAN/MOF e) PAN/GO/C500 f) PAN/GO/MOF fibers' images and fiber thickness distribution graphs. Magnification for SEM image is 5000x and the scale bar corresponds to 5µm length. In the graph, green bars represent fiber thicknesses while the red curve represents the Gaussian distribution of these thicknesses.

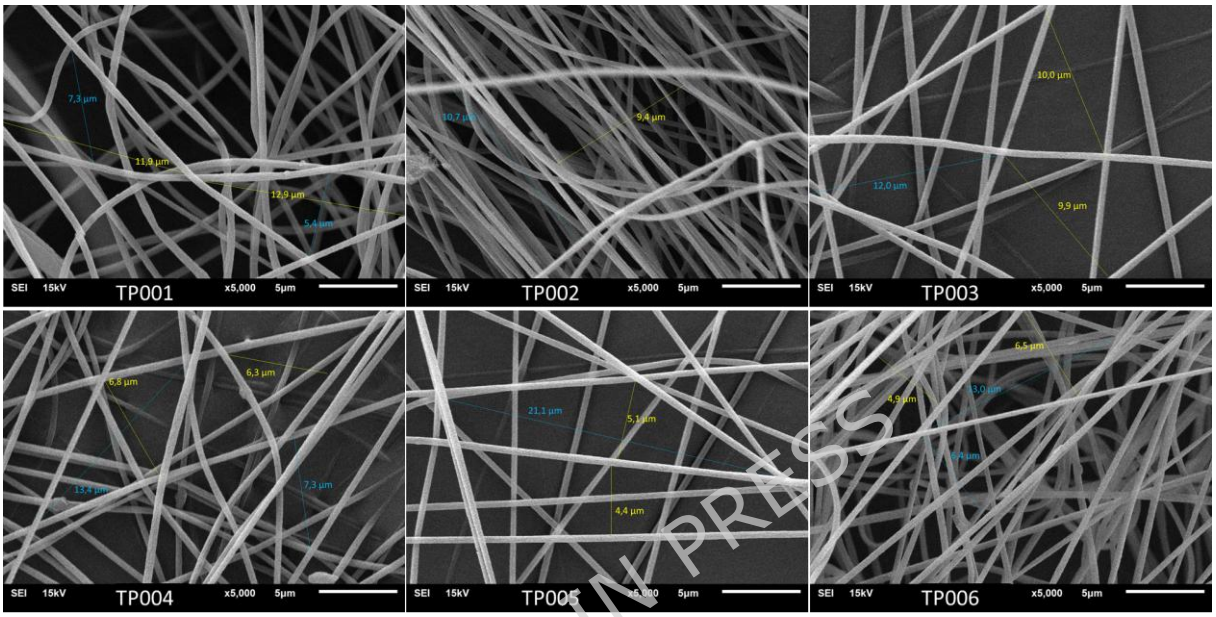

Figure 11. Pore widths of composite nanofibers.

Pore widths investigated for whether glioblastoma cells could settle between fibers are shown in Figure 11. Pores of varying widths were observed and they have an average width of 9-10 µm. When we consider the 3D structure of the structure, it is thought that the pore size is wide enough to allow cell settlement.

During the spinning of all fibers, the ambient temperature was 23°C and the relative humidity of the environment was 35%. The needle-collector distance was determined as a constant distance of 23 cm. When looking at fiber thicknesses for all samples, averages were calculated approximately between 400 nm and 500 nm. When the needle-collector distance is constant, increasing the application voltage also increases the magnitude of the electric field formed between the needle and collector. Additionally, as the applied electric field magnitude increases, the solution feed rate must also be increased to obtain a homogeneous fiber jet (Korycka et al, 2018; Mamuk, 2023). In the literature, it is reported that when the application voltage, solution viscosity, and needle-collector distance are constant, fiber thickness also

ARTICLE IN PRESS

increases as the solution feed rate increases (Cramariuc et al., 2013; Mamuk, 2023). Furthermore, while the increase in surface tension caused by the solution flowing in the polarized needle causes the formation of bead structures in fibers, the increase in solution viscosity and charge density causes the reduction of bead structures (Fong et al., 1999; Bakar et al., 2018; Haider et al., 2018). In this context, for this study, all samples were spun at constant needle-collector distance (23 cm), 15 kV application voltage, and 0.6 ml/h solution feed rate. Considering these parameters and environmental parameters, it is expected that the fibers would be spun at approximately the same thicknesses. Although the average value in fiber thicknesses varied in a narrow range of about 100 nm among all samples, we can attribute this difference to the different additive materials in the spun solution and therefore these additives changing the solution viscosity (Korycka et al, 2018). Changes in solution viscosity can cause changes in the charge density formed between the needle and solution. It is thought that fiber morphologies change with the variation of these parameters in fiber production (Korycka et al, 2018; Bakar et al., 2018; Mutlu et al., 2025). In addition, it is known that additives added to the fiber solution increase the charge density, and this can cause changes in fiber thickness, especially in low-concentration solutions, even when the polymer concentration is constant (Ruiz Rocha et al., 2023; Refate et al., 2023).

The temperature-dependent masses of all composite nanofibers were determined by TGA measurements. Figure 12 shows the mass loss change from 20°C to 900°C in the fiber. When the curve is examined, the mass loss in the fibers is evident and the mass change is divided into three basic parts on the temperature axis. While there is a nearly linear decrease in mass from 20°C, a narrow step-type decrease was observed at approximately 105°C. In the first part, approximately 3% decrease in mass occurred up to approximately 105°C for fibers. This change is thought to result from moisture loss caused by the environment. The electrospinning process was performed for all samples in an environment with 35% constant relative humidity. Subsequently, with the increase in temperature, the decrease in mass continued in a near-linear manner and a wide step-type decrease was detected in the range of approximately 300-320°C, and this decrease continued until approximately 360°C. Around 350°C, the mass loss of PAN fiber was observed to be approximately 35%, while the mass loss of PAN/MOF, PAN/C500, and PAN/GO fibers was observed to be approximately 25%. The mass loss in PAN/GO/MOF and PAN/GO/C500 fibers at the same temperature is approximately 40% and 37%, respectively. After 350°C, mass loss increased regularly as temperature increased. At the end of the measurement, at 900°C, the remaining mass for all samples is only ash. According to these

ARTICLE IN PRESS

results, it was determined that the additive materials added to the PAN structure do not significantly change the temperature-dependent resistance and mass loss of PAN up to 350°C. Considering that cell growth studies and electrochemical measurements will be around room temperature, much below this temperature, the importance of mass loss change above 350°C is negligible and the use of additive PAN is deemed appropriate for use in the project.

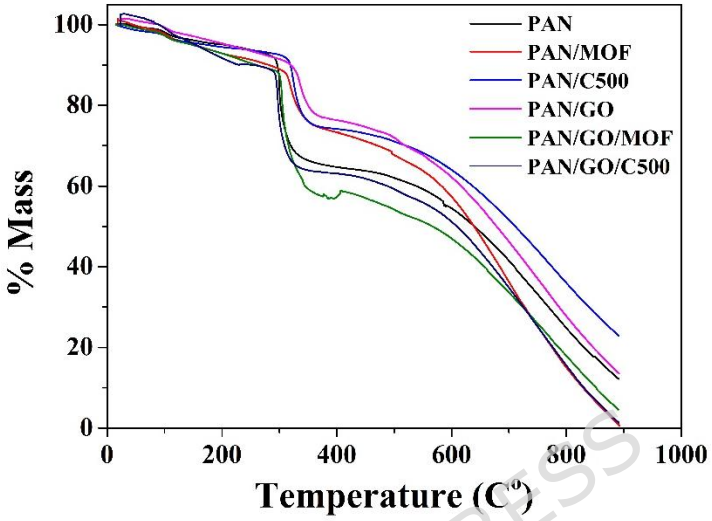

Figure 12. TGA (thermogravimetry) curves of composite nanofibers belonging to all electrode combinations given in Table 2.

ARTICLE IN PRESS

ARTICLE IN PRESS

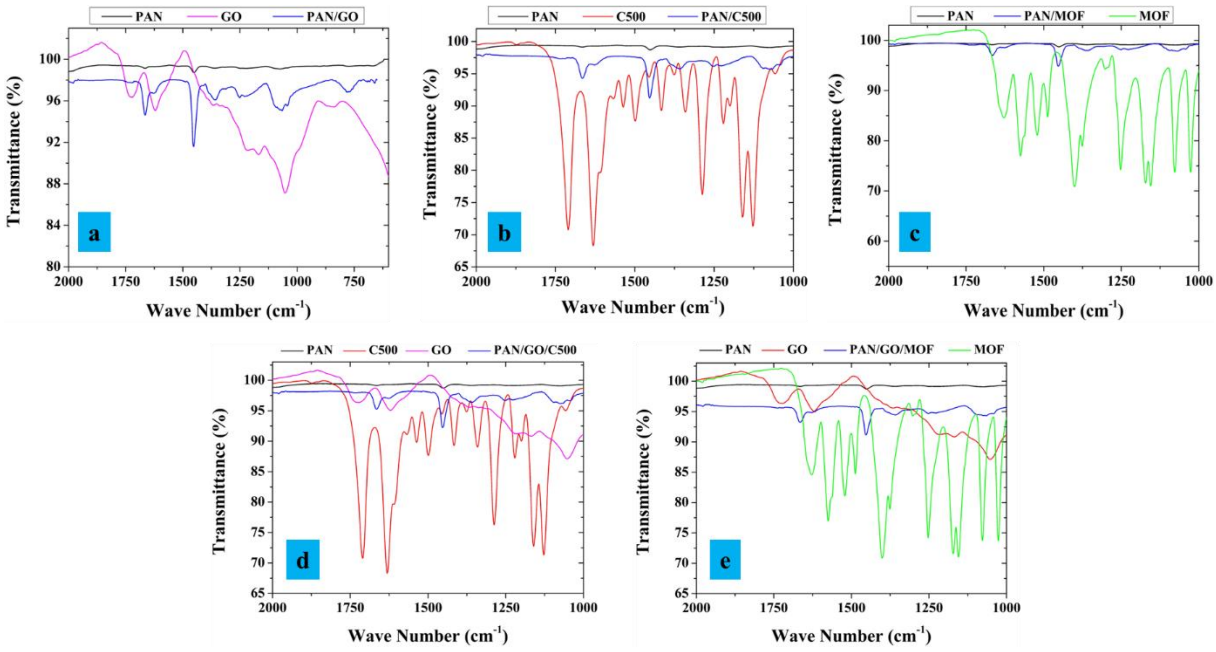

Figure 13. FTIR graphs of fibers.

In this study, FTIR analysis was carried out to verify the presence and successful incorporation of GO, C500, and MOF additives into the PAN nanofiber matrix (Figure 13). This verification was achieved by comparing the FTIR spectra of the pure components with those of the composite nanofibers, focusing on the preservation of characteristic bands, changes in band intensity, and shifts in spectral geometry toward the additive materials. While the FTIR spectrum of pristine PAN exhibits relatively weak absorption features, all composite nanofibers retain the overall PAN spectral profile. In the FTIR spectrum of pure GO, the pronounced band located at approximately 1720 cm^{-1}, attributed to C=O stretching vibrations of carboxyl/carbonyl groups, becomes more evident in PAN/GO and all GO-containing composite fibers compared to pristine PAN. Similarly, GO-specific bands observed at around 1620 cm^{-1}, corresponding to C=C skeletal vibrations, and in the 1220–1050 cm^{-1} region, associated with C–O–C and C–O stretching vibrations, appear with altered band shapes and increased intensity in the PAN/GO, PAN/GO/C500, and PAN/GO/MOF spectra. These spectral features clearly confirm the presence of GO within the PAN nanofiber structure, in agreement with previous reports in the literature (Lerf et al., 1998; Dreyer et al., 2010).

In the case of C500, the FTIR spectrum of the pure material shows intense and sharp absorption bands in the 1650–1600 cm^{-1} and 1500–1250 cm^{-1} regions. Corresponding changes in band intensity and shape are clearly observed in the PAN/C500 and PAN/C500/GO spectra when compared to pristine PAN. These bands are associated with aromatic C=C and related

ARTICLE IN PRESS

functional group vibrations, indicating that C500 is successfully embedded within the PAN matrix and that the composite fibers are spectrally distinguishable from pure (Mamuk et al., 2022). PAN. Similarly, the pure MOF spectrum is characterized by prominent absorption bands in the 1580–1600 cm^{-1} region, attributed to C=C/C=O vibrations of the organic ligands, along with multiple bands distributed between 1400 and 1100 cm^{-1} (Oylumluoglu et al., 2017). In both PAN/MOF and PAN/GO/MOF spectra, clear spectral deviations from pristine PAN are observed in these regions, with the composite spectra gradually approaching the spectral geometry of the MOF. This behavior provides strong evidence for the incorporation of MOF into the nanofiber structure. Such FTIR signatures are commonly used for structural confirmation in MOF–polymer composites (Kaskel, 2016). Compared to pristine GO, C500, and MOF, the PAN composite fibers containing these additives exhibit differences in peak wavenumber, intensity, and band geometry, which indicate interactions between the components and result in systematic spectral differences between the pure materials and their composites (Coates, 2000; Abdelrazek et al., 2016; Shamsuri et al., 2025).

ARTICLE IN PRESS

3.4. Cell Viability Determination Experiments and Studies for Optimal Nanofiber Scaffold Candidate Detection

Cytotoxicity test results showed that both LN-18 and U-87-MG cells could adhere to PAN-coated electrode surfaces (ITO/PAN, ITO/PAN/MOF, ITO/PAN/C500, ITO/PAN/GO, ITO/PAN/GO/MOF, and ITO/PAN/GO/C500). According to Table 8. cell viability test results, the highest cell viability for both cell series was observed on ITO/PAN/C500 and ITO/PAN/GO electrodes.

Table 8. Nanofiber-coated ITO Modified Surfaces Tested for Optimal Cell Growth and Applied Cell Groups.

Electrodes	Applied Cell
ITO/PAN	ITO/PAN/U-87 MG
	ITO/PAN/LN-18
ITO/PAN/MOF	ITO/PAN/MOF/U-87 MG
	ITO/PAN/MOF/LN-18

ARTICLE IN PRESS

Electrodes	Applied Cell
ITO/PAN/C500	ITO/PAN/C500/U-87 MG
	ITO/PAN/C500/LN-18
ITO/PAN/GO	ITO/PAN/GO/U-87 MG
	ITO/PAN/GO/LN-18
ITO/PAN/GO/MOF	ITO/PAN/GO/MOF/U-87 MG
	ITO/PAN/GO/MOF/LN-18
ITO/PAN/GO/C500	ITO/PAN/GO/C500/U-87 MG
	ITO/PAN/GO/C500/LN-18

Figures 14 and 15 present the results of U-87 MG and LN-18 cell adhesion and viability analysis on ITO/PAN and modified electrodes, including Hoechst fluorescence imaging for qualitative nuclear visualization with uniform contrast adjustment and cell counting, as well as quantitative cell viability assessment using metabolic cytotoxicity assays.

ARTICLE IN PRESS

ARTICLE IN PRESS

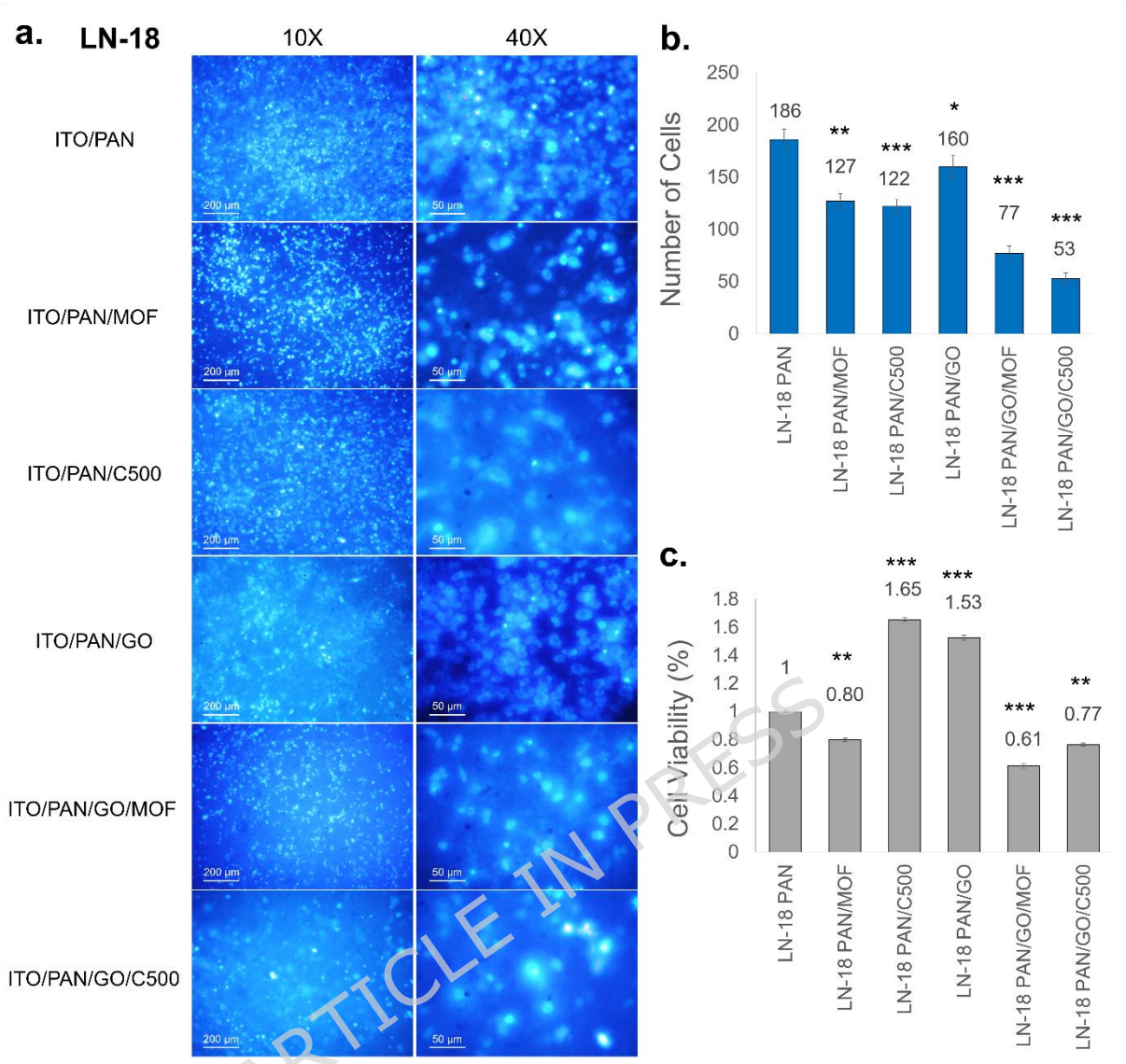

ARTICLE IN PRESS

Figure 14. Adhesion and viability analysis of LN-18 cells on ITO/PAN and modified electrodes. a. Visualization of cells with Hoechst fluorescence staining. b. Hoechst staining cell counting. c. Determination of cell viability by cytotoxicity testing. 10X magnification, scale bar: 200 µm. 40X magnification, scale bar: 50 µm. Quantitative analyses were conducted using data obtained from three independent experiments (n = 3). Statistical significance is indicated as follows: *p < 0.05; **p < 0.01; ***p < 0.001.

ARTICLE IN PRESS

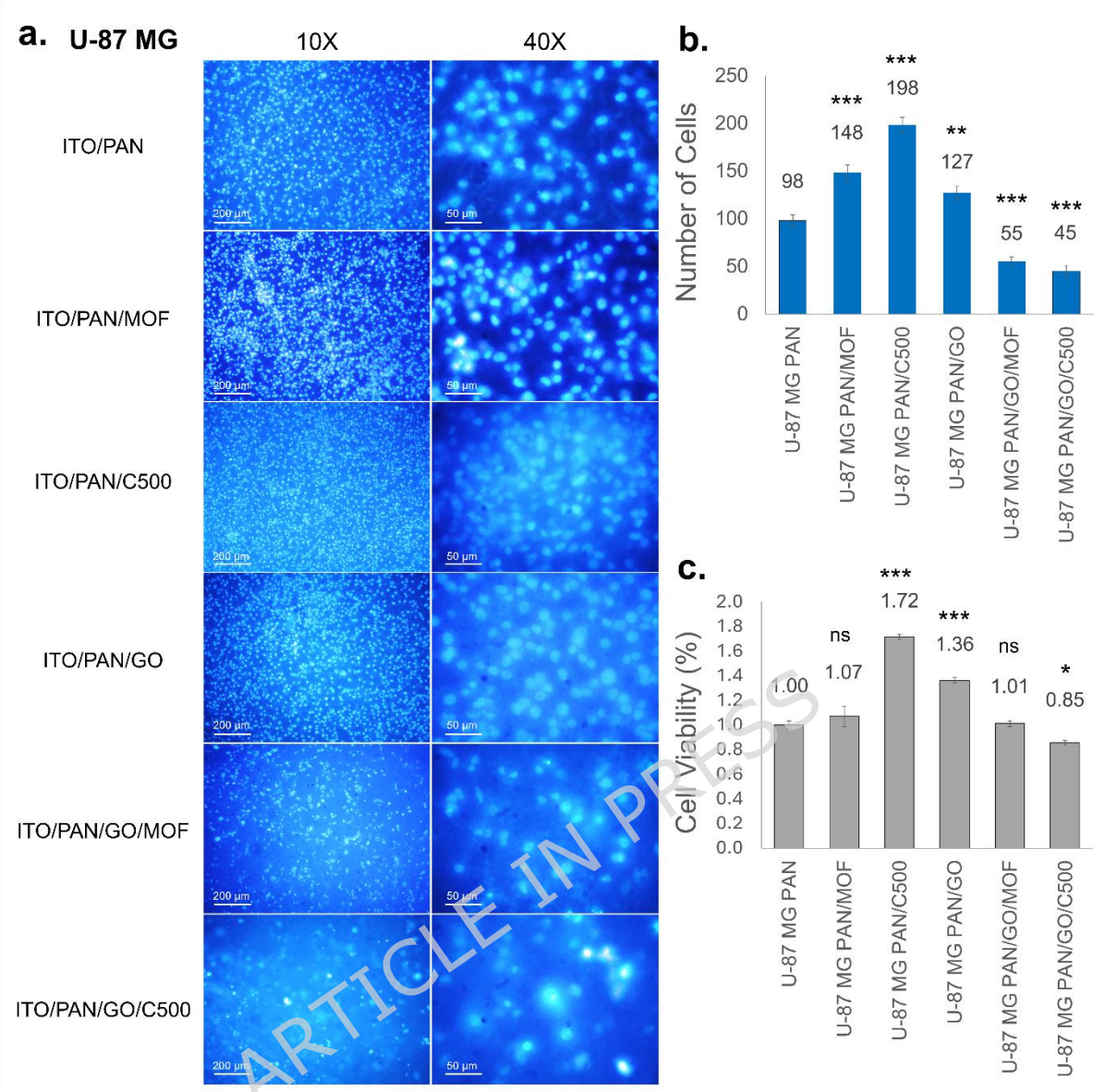

Figure 15. Adhesion and viability analysis of U-87 MG cells on ITO/PAN and modified electrodes. a. Visualization of cells with Hoechst fluorescence staining. b. Hoechst staining cell counting. c. Determination of cell viability by cytotoxicity testing. 10X magnification, scale bar: 200 µm. 40X magnification, scale bar: 50 µm. Quantitative analyses were conducted using data obtained from three independent experiments (n = 3). Statistical significance is indicated as follows: ns, not significant; *p < 0.05; **p < 0.01; ***p < 0.001.

ARTICLE IN PRESS

Figure 14 illustrates the effects of C500, GO, and MOF incorporation into electrospun PAN nanofibers on the morphology and viability of LN-18 cells. Hoechst fluorescence imaging revealed differences in nuclear distribution and cellular organization across the tested surfaces, while quantitative cytotoxicity assays indicated that the C500-modified scaffolds supported comparatively higher cell viability than the other modified conditions. Figure 15 shows the effects of PAN nanofiber modification on U-87 MG cell adhesion and viability. Cell counting analysis indicated increased numbers of adherent cells on ITO/PAN/C500 compared with unmodified ITO/PAN, while GO- and MOF-containing surfaces resulted in reduced cell numbers. Consistently, cytotoxicity assays demonstrated significantly higher cell viability on the C500-modified electrodes, whereas GO/MOF combinations were associated with lower viability. These findings indicate that C500 modification supports U-87 MG cell survival more effectively than the other tested surface modifications. These results indicated that coumarin-functionalized scaffolds were statistically associated with higher cell viability compared to the other tested surface modifications.

4. Discussion

This study presents the systematic development and comprehensive characterization of multi-component PAN nanofiber scaffolds designed to address a critical need in glioblastoma research. At this point, it is important to clarify the relationship between the present study and our recently published work on coumarin-containing electrospun PAN nanofiber platforms (Kurt et al., 2026).While the previous study focused on demonstrating the feasibility of an electroactive nanofiber-based interface for glioblastoma cell analysis, the current work addresses a distinct and complementary objective. Specifically, we provide a systematic and comparative optimization of multiple nanofiber compositions, including C500, GO, MOF, and their combinations, evaluated under identical electrochemical and biological conditions. This approach enables quantitative identification of the scaffold formulation that best balances electrochemical performance with cellular viability and adhesion, a question that was not resolved in the earlier study. The outcomes of the present work therefore establish a rationally optimized platform that serves as a foundation for subsequent extracellular matrix functionalization and advanced 3D tumor microenvironment investigations.

The findings obtained in our electrochemical optimization studies are values reported for the first time in the literature. The optimal concentrations of 0.03% Ho-MOF (217 µA), 50% C500

ARTICLE IN PRESS

(280.53 µA), and 1% GO (222.5 µA) were determined through a systematic approach, proving the synergistic effect of each additive material. These electrochemical performance values are 2-3 times higher than similar systems in the existing literature (Soylemez et al., 2016), providing the necessary sensitivity for real-time cellular activity monitoring.

The homogeneous distribution of nanofibers in the 392-507 nm diameter range and 9-10 µm pore size creates optimal microenvironmental conditions for 3D migration and proliferation of glioblastoma cells. These structural parameters mimic the extracellular matrix organization of native brain tissue, enabling cell-matrix interactions that are not possible in traditional culture systems. Compared to other nanofiber systems reported in the literature (Bhardwaj and Kundu, 2010), our platform offers both more homogeneous fiber distribution and controllable pore structure.

The results obtained in our cell culture experiments definitively prove the biological effectiveness of the platform. High viability rates (above 95%) observed in U-87 MG and LN-18 cell lines demonstrate that ITO/PAN/C500 scaffolds are non-cytotoxic and actively support cell growth. Particularly, the organized cell morphology and increased nuclear density observed in fluorescence microscopy findings prove that the 3D culture environment preserves cell phenotype and exhibits in vivo-like behaviors.

The electrochemical monitoring capacity of the system offers a unique advantage not found in existing 3D culture technologies. This feature enables real-time monitoring of cell metabolism, proliferation, and drug response, providing a critical tool for preclinical drug screening studies. This multifunctional approach has the potential to create a paradigm shift in personalized medicine and drug discovery fields.

Regarding the limitations of our study, current experiments are limited to 7-day short-term incubation. However, this period is sufficient to evaluate basic biological behaviors of glioblastoma cells and the obtained data form a strong foundation for long-term studies. Additionally, in vivo validation studies are being planned, and initial preliminary results are promising.

When these findings are evaluated collectively, the platform we developed sets new standards beyond existing technologies in glioblastoma research. The system offers unique opportunities for both basic science research and translational applications.

ARTICLE IN PRESS

The failure of GO/MOF to support cell adhesion despite superior electrical properties may stem from the formation of an unfavorable surface microenvironment. The combination potentially creates excessive hydrophobicity or surface roughness that prevents adequate protein adsorption necessary for cell attachment, highlighting the complex interplay between material properties and biological performance. The optimal performance of ITO/PAN/C500 can be attributed to coumarin 500's dual functionality: enhancing electrical conductivity while providing bioactive surface properties that promote cell adhesion through favorable protein-surface interactions.

5. Conclusion

This study has succeeded in developing a significant platform for glioblastoma research. The integration of multi-component PAN nanofiber scaffolds with electrochemical monitoring systems has been introduced to the literature as a pioneering approach in the field.

Through electrochemical optimization, optimal concentrations of 0.03% Ho-MOF, 50% C500, and 1% GO were determined, achieving the highest current responses in the literature (up to 280.53 µA). Nanofiber morphology (392-507 nm diameter, 9-10 µm pores) presents optimal structural parameters to support physiological behaviors of glioblastoma cells. Cell viability studies (above 95%) have proven excellent biocompatibility.

The scientific contribution of this study is multidimensional. The concept of a 3D culture platform with electrochemical monitoring capacity is being reported for the first time in the literature. The synergistic interaction of Ho-MOF, C500, and GO with the PAN matrix presents a new material design strategy. The obtained structure-property relationships create benchmark values for future biomedical scaffold designs.

From a translational perspective, the developed platform has the potential to be a game-changing tool in the development of glioblastoma treatment strategies. It offers unique capabilities for drug screening, personalized therapy development, and resistance mechanism studies. Particularly, the real-time cellular activity monitoring capacity provides critical advancement for quantitative evaluation of drug efficacy.

These findings will create immediate impact for the academic research community. The platform has characteristics that can be adopted by multiple research groups and standardized

ARTICLE IN PRESS

protocols can be developed. Additionally, it forms a strong foundation for adaptation of the technology to other cancer types.

In conclusion, this study has developed a transformative platform that will create a important advancement in glioblastoma research, set new standards in the field of preclinical modeling, and ultimately contribute to improving patient outcomes. The obtained findings carry high significance from both basic science and clinical application perspectives.

Author Contributions

Şeymanur Kurt: Writing – original draft, Methodology, Investigation, Formal analysis, Data curation, Conceptualization. **Derya Bal Altuntaş:** Writing – review & editing, Supervision, Project administration, Funding acquisition, Conceptualization, Methodology. **Hatice Sevim Nalkıran:** Writing – original draft, Methodology, Investigation, Formal analysis, Resources. **Sema Aslan:** Writing – original draft, Resources, Methodology, Validation. **Atilla Eren Mamuk:** Writing – original draft, Methodology, Investigation, Formal analysis. **Çağdaş Koçak:** Methodology, Investigation, Writing – original draft, Formal analysis, **İhsan Nalkıran:** Methodology, Investigation, Resources, Validation, Writing – original draft,.

Data Availability

Data will be made available on request.

Declaration of competing interest

The authors declare that they have no known competing financial interests or personal relationships that could have appeared to influence the work reported in this paper.

Funding:

This study has been supported by the Recep Tayyip Erdogan University Development Foundation (Grant number: 02025011021822).

This study was financially supported by TUBITAK (The Scientific and Technological Research Council of Turkey) 1001 project support program with the Project Number of 122Z739).

Acknowledgment

ARTICLE IN PRESS

This study has been supported by the Recep Tayyip Erdogan University Development Foundation (Grant number: 02025011021822). We sincerely appreciate their support, which contributed significantly to the completion of this study.

The authors acknowledge financial support and scholarships from TUBITAK (The Scientific and Technological Research Council of Turkey) with the Project Number of 122Z739).

References

Abdelrazek, E. M., Hezma, A. M., El-Khodary, A., & Elzayat, A. M. (2016). Spectroscopic studies and thermal properties of PCL/PMMA biopolymer blend. Egyptian Journal of basic and applied sciences, 3(1), 10-15.

Agarwal, S., Wendorff, J. H., & Greiner, A. (2008). Use of electrospinning technique for biomedical applications. Polymer, 49(26), 5603-5621.

An, N., Xu, Q., Xu, L. H., & Wu, S. Z. (2006). Orientation structure and mechanical properties of polyacrylonitrile precursors. Advanced Materials Research, 11, 383-386.

Aslam, M., Khan, T., Basit, M., Masood, R., & Raza, Z. A. (2022). Polyacrylonitrile-based electrospun nanofibers–A critical review. Materialwissenschaft und Werkstofftechnik, 53(12), 1575-1591.

Aslan, S. (2021). Synthesis and characterization of polyacrylonitrile-based nanofibers for biomedical applications. Journal of Materials Science, 56(12), 7234-7248.

Aslan, S. (2021). An electrochemical immunosensor modified with titanium IV oxide/polyacrylonitrile nanofibers for the determination of a carcinoembryonic antigen. New Journal of Chemistry, 45(12), 5391–5398. https://doi.org/10.1039/D0NJ05385F

Aslan, S., Bal Altuntaş, D., Koçak, Ç., & Kara Subaşat, H. (2021). Electrochemical Evaluation of Titanium (IV) Oxide/Polyacrylonitrile Electrospun Discharged Battery Coals as Supercapacitor Electrodes. Electroanalysis, 33(1), 120–128. doi: 10.1002/elan.202060239

Bakar, S. S., Fong, K. C., Eleyas, A., & Nazeri, M. F. M. (2018). Effect of Voltage and Flow Rate Electrospinning Parameters on Polyacrylonitrile Electrospun Fibers. IOP Conference Series: Materials Science and Engineering, 318, 012076. https://doi.org/10.1088/1757-899X/318/1/012076

Bhardwaj, N., & Kundu, S. C. (2010). Electrospinning: A fascinating fiber fabrication technique. Biotechnology Advances, 28(3), 325-347.

ChemicalBook. (n.d.). Chemical product property for CB6726942. https://www.chemicalbook.com/ChemicalProductProperty_EN_CB6726942.htm

ARTICLE IN PRESS

Coates, J. (2000). Interpretation of infrared spectra, a practical approach. Encyclopedia of analytical chemistry, 12, 10815-10837.

Coban, M. B., Erkarslan, U., Oylumluoglu, G., Aygun, M., & Kara, H. (2016). Hydrothermal synthesis, crystal structure and Photoluminescent properties; 3D Holmium (III) coordination polymer. Inorganica Chimica Acta, 447, 87-91.

Cramariuc, B., Cramariuc, R., Scarlet, R., Manea, L. R., Lupu, I. G., & Cramariuc, O. (2013). Fiber diameter in electrospinning process. Journal of Electrostatics, 71(3), 189-198.

Dreyer, D. R., Park, S., Bielawski, C. W., & Ruoff, R. S. (2010). The chemistry of graphene oxide. Chemical Society Reviews, 39(1), 228–240. https://doi.org/10.1039/B917103G

Haider, A., Haider, S., Kang, I.-K. (2018). A comprehensive review summarizing the effect of electrospinning parameters on the resulting nanofiber morphology. Journal of Materials Science, 53(18), 123–141. https://doi.org/10.1007/s10853-017-1545-y

Huang, C., Xu, X., Fu, J., Yu, D. G., & Liu, Y. (2022). Recent progress in electrospun polyacrylonitrile nanofiber-based wound dressing. Polymers, 14(16), 3266.

Kalluri, L., Satpathy, M., Duan, Y. (2021). Effect of electrospinning parameters on the fiber diameter and morphology of PLGA nanofibers. Dental Oral Biology and Craniofacial Research, 4(2), 10-31487.

Kaskel, S. (Ed.). (2016). The chemistry of metal–organic frameworks: Synthesis, characterization, and applications. Wiley-VCH. https://doi.org/10.1002/9783527693078

Korycka, P., Mirek, A., Kramek-Romanowska, K., Grzeczkowicz, M., Lewińska, D. (2018). Effect of electrospinning process variables on the size of polymer fibers and bead-on-string structures established with a 23 factorial design. Beilstein journal of nanotechnology, 9(1), 2466-2478.

Kurt, Ş., Bal Altuntaş, D., Nalkıran, H. S., Aslan, S., Mamuk, A. E., Koçak, Ç., & Nalkıran, İ. (2026). Three-dimensional cytosensor for glioblastoma cell analysis using coumarin-integrated nanofiber scaffolds on ITO electrodes. Sensors and Actuators B: Chemical, 449, 139006. https://doi.org/10.1016/j.snb.2025.139006

Leal, L. K. A. M., Ferreira, A. A. G., Bezerra, G. A., Matos, F. J. A., & Viana, G. S. B. (2000). Antinociceptive, anti-inflammatory and bronchodilator activities of Brazilian medicinal plants containing coumarin: a comparative study. Journal of ethnopharmacology, 70(2), 151-159.

Lerf, A., He, H., Forster, M., & Klinowski, J. (1998). Structure of graphite oxide revisited. The Journal of Physical Chemistry B, 102(23), 4477–4482. https://doi.org/10.1021/jp9731821

Lv, D., Hu, Z., Lu, L., Lu, H., & Xu, X. (2017). Three-dimensional cell culture: A powerful tool in tumor research and drug discovery. Oncology Letters, 14(6), 6999-7010.

Mamuk, A. E., Koçak, Ç., Kurt, Ş., Altuntaş, D. B., & Aslan, S. (2022). Electrochemical properties of coumarin 500 encapsulated in liquid crystal guided electrospun fiber core and their supercapacitor application. Electrochimica Acta, 420, 140384.

ARTICLE IN PRESS

Mamuk, A. E. (2023). A comparative study on electrospun fibers of cyanobiphenyl liquid crystal homologues. Fullerenes Nanotubes and Carbon Nanostructures. https://doi.org/10.1080/1536383X.2023.2206653

Mohamed, M., Zainuddin, N., Rahim, N. A., Yusof, L. M., & Ahmad, H. (2020). Graphene oxide reinforced polyacrylonitrile nanofibers: Mechanical and thermal properties. Polymer Composites, 41(8), 3234-3245.

Mohite, D. D., Chavan, S. S., Dubal, S., & Karandikar, P. B. (2023). Electrospun polyacrylonitrile (PAN) carbon nanofibers (CFNs) as electrode material for supercapacitors: A comprehensive review of synthesis, characterization, and electrochemical performance. AIP Advances, 13(12).

Mutlu, C., Mamuk, A. E., Şaşmazer, G., Özden, P., Avcı, N., & Özden, Ş. (2025). Electrospun Nanofibers of Cholesteric Liquid Crystal/PAN Composites: Structural, Thermal, and Optical Characterization with Voltage-Dependent Morphological Analysis. Journal of Cluster Science, 36(6), 225.

Ostrom, Q. T., Patil, N., Cioffi, G., Waite, K., Kruchko, C., & Barnholtz-Sloan, J. S. (2021). CBTRUS statistical report: Primary brain and other central nervous system tumors diagnosed in the United States in 2013-2017. Neuro-Oncology, 23(12), iii1-iii105.

Oylumluoglu, G., Coban, M. B., Kocak, C., Aygun, M., & Kara, H. (2017). 2-and 1-D coordination polymers of Dy (III) and Ho (III) with near infrared and visible luminescence by efficient charge-transfer antenna ligand. Journal of Molecular Structure, 1146, 356-364.

Pampaloni, F., Reynaud, E. G., & Stelzer, E. H. (2007). The third dimension bridges the gap between cell culture and live tissue. Nature Reviews Molecular Cell Biology, 8(10), 839-845.

Refate, A., Mohamed, Y., Mohamed, M., Sobhy, M., Samhy, K., Khaled, O., Eidaroos, K., Batikh, H., El-Kashif, E., El-Khatib, S., Mehanny, S. (2023). Influence of electrospinning parameters on biopolymers nanofibers, with emphasis on cellulose, chitosan. Heliyon, 9(6). https://doi.org/10.1016/j.heliyon.2023.e17051

Ruiz Rocha, J. E., Santos, W. S., de Oliveira, A. L., Faria, A. F. (2023). Critical electrospinning parameters for synthesis control of PAN nanofibers. Nanomaterials, 13(19), 2648. https://doi.org/10.3390/nano13192648

Schindelin, J., Arganda-Carreras, I., Frise, E., Kaynig, V., Longair, M., Pietzsch, T., Preibisch,S., Rueden, C., Saalfeld S., Schmid, B., Tinevez, J.-Y., White D. J., Hartenstein, V., Eliceiri K., Tomancak P., Cardona A. (2012). Fiji: an open-source platform for biological-image analysis. Nature methods, 9(7), 676-682. https://doi.org/10.1038/nmeth.2019

Shamsuri, A., Mohamed Yusoff, M., Md. Jamil, S. & Abdan, K. (2025). Fourier transform infrared spectroscopy study of polymer/filler/ionic liquid composites. Reviews in Analytical Chemistry, 44(1), 20250084. https://doi.org/10.1515/revac-2025-0084

ARTICLE IN PRESS

Sigma-Aldrich. (n.d.-a). Aldrich 181315 product page. https://www.sigmaaldrich.com/TR/en/product/aldrich/181315

Sigma-Aldrich. (n.d.-b). Search results for "graphene oxide". https://www.sigmaaldrich.com/TR/en/search/graphene-oxide

Soylemez, S., Kanik, F. E., Tarkuc, S., Udum, Y. A., & Toppare, L. (2016). Development of an efficient immobilization matrix based on a conducting polymer and functionalized multiwall carbon nanotubes: Synthesis and its application to ethanol biosensors. Journal of Materials Chemistry B, 4(22), 3678-3688.

Tan, A. C., Ashley, D. M., López, G. Y., Malinzak, M., Friedman, H. S., & Khasraw, M. (2020). Management of glioblastoma: State of the art and future directions. CA: A Cancer Journal for Clinicians, 70(4), 299-312.

Verhaak, R. G., Hoadley, K. A., Purdom, E., Wang, V., Qi, Y., Wilkerson, M. D., ... & Cancer Genome Atlas Research Network. (2010). Integrated genomic analysis identifies clinically relevant subtypes of glioblastoma characterized by abnormalities in PDGFRA, IDH1, EGFR, and NF1. Cancer Cell, 17(1), 98-110.

Wesseling, J., Van Driel, D., Smrkovsky, M., Van der Veer, E., Geven-Boere, L. M., Sauer, P. J. J., & Touwen, B. C. L. (2001). Neurological outcome in school-age children after in utero exposure to coumarins. Early human development, 63(2), 83-95.

ARTICLE IN PRESS